Journal Pre-proof

Naïve antibody library derived monoclonal antibody against VP35 of Ebola virus

Jing Yi Lai, Angela Corona, Chong Lee Ng, Enzo Tramontano, Yee Siew Choong, Theam Soon Lim

PII: S0141-8130(23)02465-0

DOI: https://doi.org/10.1016/j.ijbiomac.2023.125571

Reference: BIOMAC 125571

To appear in: *International Journal of Biological Macromolecules*

Received date: 3 April 2023

Revised date: 13 June 2023

Accepted date: 24 June 2023

Please cite this article as: J.Y. Lai, A. Corona, C.L. Ng, et al., Naïve antibody library derived monoclonal antibody against VP35 of Ebola virus, *International Journal of Biological Macromolecules* (2023), https://doi.org/10.1016/j.ijbiomac.2023.125571

Naïve antibody library derived monoclonal antibody against VP35 of Ebola virus

Jing Yi Lai[a], Angela Corona[b], Chong Lee Ng[a], Enzo Tramontano[b], Yee Siew Choong[a], Theam Soon Lim[a,c]*

[a] Institute for Research in Molecular Medicine, Universiti Sains Malaysia, 11800 Penang, Malaysia

[b] Department of Life and Environmental Science, University of Cagliari, 09042 Monserrato, Italy

[c] Analytical Biochemistry Research Centre, Universiti Sains Malaysia, 11800 Penang, Malaysia

*To whom correspondence should be addressed:

Tel: +604-653-4852, Fax: +604-653-4803, Email: theamsoon@usm.my

Abstract

Ebola virus is notorious for causing severe and even deadly haemorrhagic fever in infected humans and non-human primates. The high fatality rate of Ebola virus disease (EVD) has highlighted the need for effective diagnosis and treatment. Two monoclonal antibodies (mAbs) have been approved by USFDA for treatment of EVD. Virus surface glycoprotein is the common target for diagnostic and therapy including vaccines. Even so, VP35, a viral RNA polymerase cofactor and interferon inhibitor could be a potential target to curb EVD. The present work describes the isolation of three mAb clones from a phage-displayed human naïve scFv library against recombinant VP35. The clones showed binding against rVP35 *in vitro* and inhibition of VP35 in luciferase reporter gene assay. Structural modelling analysis was also carried out to identify the binding interactions involved in the antibody-antigen interaction model. This allows some insight into the "fitness" of the binding pocket between the paratope and target epitope which would be useful for the design of new mAbs through *in silico* means in the future. In conclusion, the information obtained from the 3 isolated mAbs could be potentially useful in the quest to improve VP35 targeting for therapeutic development in the future.

Keywords: phage display; Ebola; VP35; naïve library; scFv; *Leishmania tarentolae*

1. Introduction

Ebola virus disease (EVD) is one of the deadliest viral infections in human and non-human primates characterized with haemorrhagic fever which might eventually lead to multiorgan failure and death. Although the outbreaks of EVD mainly occurs in Africa, healthcare communities and researchers remain vigilant due to the high mortality rate. EVD is caused by *Ebolavirus* that is first discovered in 1976 at Democratic Republic of Congo [1]. *Ebolavirus* is classified under the family *Filoviridae,* containing six species in the genus, namely *Zaire ebolavirus* (EBOV), *Sudan ebolavirus* (SUDV), *Tai Forest ebolavirus* (TAFV), *Bundibugyo ebolavirus* (BDBV), *Reston ebolavirus* (RESTV), and *Bombali ebolavirus* (BOMV) [2, 3]. Among the six species, only EBOV, SUDV, TAFV and BDBV are clinically significant to human, while EBOV is responsible for majority of the EVD outbreaks to date [4]. Hence, most of the research activities are centred around EBOV, including a vaccine [5, 6] and two monoclonal antibodies therapies that are among the most promising therapeutic agents to treat EVD [7].

EBOV is a single-stranded, negative-sense RNA virus. The viral RNA genome contains seven genes encoded for nucleoprotein (NP), polymerase cofactor (virion protein (VP) 35), matrix protein (VP40), glycoprotein (GP), transcription activator (VP30), minor matrix protein (VP24), and RNA-dependent RNA polymerase (L) [4]. The *GP* gene is multicistronic and transcribes three proteins, including a full-length membrane glycoprotein (GP) and two secretory glycoprotein (soluble GP (sGP) and small soluble GP (ssGP)) [4]. GP is commonly identified as the main therapy target as it mediates attachment and entry of the virus to the host cell, and activation of pro-inflammatory responses [8]. Blocking of the viral GP would therefore inhibit the infection in the early stages of infection. In fact, the approved vaccine (ERVEBO) and mAbs (Inmazeb and Ebanga) are designed to target the EBOV GP [6,

9]. Nonetheless, the multifunctional protein, VP35 is also identified as an important virulence factor of EBOV.

VP35 is a cofactor of the viral RNA polymerase (L) that possess NTPase and helicase-like activities [10], and is also involved in viral assembly [11]. VP35 is a double stranded RNA (dsRNA) binding protein that interferes the activation of host's cell interferon (IFN)-inducible dsRNA and Dicer-dependent protein kinase R. It also blocks the phosphorylation of IRF-3 in RIG-1 pathway and consequently leading to the impairment of host's antiviral immune responses [12, 13]. Hence, VP35 could be another important target for EVD therapy [14] since it has been shown that a VP35 mutant EBOV does not cause lethal infection and instead elicits adaptive immune responses that can protect animals from wild-type EBOV challenge [15]. In recent years, several reports of the isolation of human monoclonal antibodies against VP35 using phage display technology has also been reported [16, 17].

Monoclonal antibody (mAb) is a class of therapeutic drug that has revolutionized the treatment approach of many diseases, including viral infections like EVD. In 2020, the U.S. Food and Drug Administration (USFDA) announced the approval of Inmazeb, the first antibody treatment for *Zaire ebolavirus* infection. Inmazeb is essentially a cocktail of three antibodies (atoltivimab, maftivimab and odesivimab) developed using transgenic mice by Regeneron Pharmaceuticals [18]. The second monoclonal antibody approved for EVD is Ebanga from Ridgeback Biotherapeutics. Ebanga, also known as Ansuvimab, was developed from B-cells of a EVD survivor [19]. As transgenic mice technology and EVD survivors are not readily available, an attractive alternative for antibody development would be the use of display technologies like phage display.

Phage display technology has been used for rapid isolation of monospecific and reproducible recombinant mAbs [20]. In brief, antibody genes are amplified from B-cells using polymerase chain reaction (PCR) and cloned into phagemid in random combination to achieve a diverse repertoire. The source of antibody genes determines the type of the library generated: naïve library is constructed from healthy and uninfected donors while immune library is generated from infected or immunized donors. A naïve library is highly diverse in theory, thus allowing it to isolate mAbs against virtually any target. Although the affinity might be lower when compared to immune libraries, this does not discount the use of naïve libraries as clones isolated from naïve libraries could be improved through affinity maturation [21]. There are many formats of recombinant antibodies but the common format used is mainly single-chain variable fragment (scFv) which retains the antigen binding site of heavy chain variable (VH) and light chain variable (VL) linked together by a short peptide linker. scFv is smaller in size and demonstrated advantages in term of ease of expression and better penetration to tissue [22].

In this study, selection of mAbs against EBOV VP35 from a diverse human naïve scFv library was attempted through biopanning and the isolated clones were characterized. The antibodies were also evaluated on a luciferase reporter gene assay for inhibition of the VP35 immunosuppressing function. The antibodies were further characterized using bioinformatic modelling to ascertain antibody-antigen interaction properties. The ability to identify clones from a naïve library highlights the flexibility of the library.

2. Materials and methods

2.1 Recombinant VP35 protein (rVP35) expression and purification

pET-45b(+) plasmid carrying EBOV VP35 gene [23] was transformed to *Escherichia coli* C41(DE3) (Lucigen). A colony was grown overnight at 37°C, 200 rpm in 5 mL of 2×YT medium (16 g tryptone, 10 g yeast extract, 5 g NaCl per litre) supplemented with 2% (w/v) glucose and 100 µg/mL of ampicillin (2×YT-amp/glu). On the next day, the overnight culture was inoculated in 500 mL of 2×YT supplemented with 0.1% (w/v) glucose and 100 µg/mL of ampicillin. The culture was grown at 37°C, 200 rpm until OD_{600nm} of 0.6 before induced with isopropyl β-D-1-thiogalactopyranoside (IPTG) at 1 mM final concentration. The induced culture was continued to culture overnight at 25°C, 160 rpm before harvest at 8000 × *g* for 10 minutes (min) at 12°C.

The harvested cell pellet was resuspended in 15 mL lysis buffer (50 mM NaH_2PO_4, 300 mM NaCl, 10 mM imidazole, pH 7.4) with 20 µg/mL of lysozyme and incubated on ice for 1 hour (h). The cell suspension was sonicated and subsequently centrifuged at 10000 × *g* for 10 min at 12°C. The lysate was removed, and the pellet was lysed with 5 mL urea buffer (100 mM NaH_2PO_4, 10 mM Tris-HCl, 8M urea, pH 8.0) for 1 h at room temperature (RT). The cell suspension was subsequently centrifuged at 10000 × *g* for 10 min. The supernatant was loaded to 1 mL Ni-NTA agarose (QIAGEN) pre-equilibrated with binding buffer (50 mM NaH_2PO_4, 300 mM NaCl, 1 mM 2-mercaptoethanol, 10% glycerol, 20 mM imidazole, pH 7.0), and incubated with rotation at RT for 1 h. The column was washed with 30 mL of wash buffer (50 mM NaH_2PO_4, 300 mM NaCl, 1 mM 2-mercaptoethanol, 10% glycerol, 70 mM imidazole, pH 7.0) and eluted with elution buffer (50 mM NaH_2PO_4, 300 mM NaCl, 1 mM 2-mercaptoethanol, 10% glycerol, 1 M imidazole, pH 7.0). Eluate collected at 1 mL fraction was analysed on 12% SDS-PAGE and validated with western blot before proceeding to biopanning. The protein concentration was determined using Bradford assay.

2.2 Biopanning on rVP35

Naïve Human AntibodY LibrarY (HAYLY) ver 2.0 [24] was used for screening of monoclonal antibodies against rVP35 protein. The panning was carried out as described previously with some modifications [24]. 10 µg of rVP35 protein (reduced to 5 µg for round 2 panning) was diluted in 100 µL of coating buffer (15 mM Na_2CO_3, 35 mM $NaHCO_3$, pH 9.4) and coated overnight in 4°C on Corning 96-well clear polystyrene high bind Stripwell™ microplate. On the next day, the antigen-coated well was washed three times with PBST (phosphate buffered saline, pH 7.4 containing 0.1% (v/v) Tween 20) and blocked with PTM (2% (w/v) skimmed milk in PBST) for 1 h at RT with gentle agitation. In parallel, another well blocked overnight with PTM was used for phage pre-incubation. 10^{11} cfu of library phage was diluted in 100 µL of PBS (or 100 µL of amplified phage for round 2 panning) and incubated with 100 µL of PTM for 1 h at RT with gentle agitation. After three PBST wash, the phage mixture was transferred to the antigen-coated well for binding at RT for 2 h with gentle agitation. The well was washed 10 times with PBST (increased to 20 washes for round 2 panning) and bound phages were eluted with 100 µL of trypsin (10 µg/mL) at 37°C for 30 min. The eluted phages were used to infect 100 µL of TG1 (Lucigen) at exponential growth phase (OD_{600nm} = 0.5) for 30 min at 37°C. Ampicillin (final concentration 100 µg/mL) and glucose (final concentration 2% (w/v)) were added to the culture and subsequently grown for 2 hr at 37°C with shaking. 10^9 cfu of M13KO7 helper phage were added to infect the cells for 30 min at 37°C. The culture was then pelleted down and resuspended with 220 µL of 2×YT medium containing 100 µg/mL of ampicillin and 60 µg/mL of kanamycin (2×YT-amp/kan). The culture was grown overnight at 30°C with constant shaking. On the next day, the culture was pelleted down and the supernatant containing phages were collected for subsequent round of panning and polyclonal ELISA.

2.3 Polyclonal phage ELISA

After two rounds of panning, the amplified phages were analysed with polyclonal ELISA. rVP35 were coated as described above. In parallel, additional wells were coated with same amount of bovine serum albumin (BSA) to serve as background control. On the next day, the wells were blocked with PTM for 1 h at RT with shaking. After three PBST wash, 50 µL of phages were diluted with 50 µL of PTM and added to the well for binding at RT for 1 h with shaking. The wells were washed three times with PBST and subsequently incubated for 1 h at RT with 100 µL of anti-M13 horseradish peroxidase (HRP) (1:5000 dilution in PTM). The wells were then washed three times with PBST and developed with 100 µL of 2,2'-azino-bis(3-ethylbenzothiazoline-6-sulfonic acid) diammonium salt (ABTS). The wells were incubated in dark with shaking and the absorbance at OD_{405nm} were measured within 30 min.

2.4 Monoclonal scFv isolation

10 µL of the rescued phages were serial diluted and used to infect XL1-Blue MRF' (Agilent Technologies) (OD_{600nm} = 0.5) at 37°C for 30 min. The infected cells were plated out on 2×YT-amp/glu agar plate. 92 single colonies were picked to inoculate 200 µL of 2×YT-amp/glu and grown overnight at 37°C with shaking. On the next day, 10 µL of the overnight culture were used to inoculate 190 µL of 2×YT-amp/glu and culture for 2 h at 37°C with shaking. 10 µL of M13KO7 (10^9 cfu) were added to infect the cell at 37°C for 30 min. The culture was pelleted down and resuspended with 220 µL 2×YT-amp/kan and grown overnight at 30°C with shaking. On the next day, the culture was pelleted and the phage containing supernatant was collected for phage ELISA using method as described for polyclonal phage ELISA (section 2.3). Clones that showed binding to the rVP35 were

analysed with colony PCR and the sequences were confirmed with sequencing. The sequence of the clones was analysed on IMGT/V-QUEST bioinformatic tool [25, 26].

2.5 Soluble scFv expression and purification in *Escherichia coli*

scFv clones were transformed to *E. coli* HB2151 (Agilent Technologies) or SHuffle T7 (NEB) and plated out on 2×YT amp/glu agar plate. 100 mL of scFv were expressed as described in section 2.1. On the next day, the culture was harvested at 10000 × g, 10 min. For clone G3, the pellet was resuspended with 2 mL of ice-cold periplasmic extraction buffer (0.2 M Tris-HCl, 0.5 mM EDTA, 0.5 M sucrose, pH 8.0) followed with 3 mL of ice-cold diluted periplasmic extraction buffer (1:5 dilution) and incubated on ice for 1 h before pelleted down at 10000 × g, 10 min. For A2 and A5, the proteins were isolated using the protocol as described in section 2.1. For all the extracted protein, the supernatant was collected and added to 1 mL of Ni-NTA resin pre-equilibrated with binding buffer (20 mM NaH_2PO_4, 500 mM NaCl, 20 mM imidazole, pH 7.4). After 1 h incubation on rotator, the resin was washed with 20 mL of binding buffer and eluted at 1 mL fraction with elution buffer (20 mM NaH_2PO_4, 500 mM NaCl, 500 mM imidazole, pH 7.4). The eluate was analysed on 12% SDS-PAGE. The protein concentration was determined using Bradford assay.

2.6 Soluble scFv expression and purification in *Leishmania tarentolae*

scFv clones were subcloned to pLTEX-5.2 plasmid modified from pLTEX-5 [27] for expression in *Leishmania tarentolae* strain P10 (Jena Bioscience). First, pLTEX-5.2 was constructed by replacing the 6xHis-tag with His-myc-tag amplified from pLABEL. His-myc-tag was cloned into pLTEX-5 at NheI and NotI restriction site. Subsequently, the scFv gene sequence were amplified and cloned into pLTEX-5.2 at NcoI and NheI restriction site.

After subcloning, transfection and clonal selection were carried out as described in manufacturer's protocol. Briefly, 200 ng of linearized plasmid were electroporated to *L. tarentolae* cells (OD_{600nm} = 1.0) at 450 V and 450 µF. Positive transfectants were selected on LEXSY BHI agar plate supplemented with 100 µg/mL of nourseothricin (NTC) and incubated at 26°C for 5 to 7 days until defined colonies appeared. Single colony was picked to inoculate 0.2 mL of LEXSY BHI medium supplemented with 100 µg/mL NTC. The culture was expanded to 1 mL NTC-supplemented BHI after 24 h and subsequently expanded to 10 mL after 48 h. For large scale expression, 100 mL of LEXSY BHI medium was inoculated with a dense starter culture (starting OD_{600nm} = 0.2) and allowed to grow at 26°C, 130 rpm for 48 h to 72 h. The culture was harvested at 1500 × g, 20 min and the supernatant was re-centrifuged at 2500 × g, 10 min to remove any remaining cells. The supernatant was diluted 1:1 with PBS and subjected to purification using Ni-NTA resin as described above. Purified scFv proteins were analysed with 12% SDS-PAGE, followed by concentration quantification with Bradford assay.

2.7 ELISA

For titration ELISA, 1 µg of rVP35 protein was coated as described in 2.2. On the next day, the wells were washed three times with PBST and blocked with PTM for 1 h at RT with gentle agitation. The wells were subsequently washed three times with PBST followed by binding of scFv (10 µg or two-fold serial dilutes) at RT for 2 h with gentle agitation. The wells were washed three times and incubated with anti-c-myc HRP (1:5000 dilution in PTM) for 1 h at RT with gentle agitation. The binding was detected with ABTS incubated in dark for 30 min. The absorbance reading at OD_{405nm} was recorded. The ELISA was performed in triplicate and plotted as mean and standard deviation.

For specificity testing, 5 µg of rVP35, BSA, ubiquitin, enhanced green fluorescent protein (EGFP) and HSP16.3 proteins were coated. The ELISA was carried out using the same method as above. 10 µg of scFvs were used for binding. The BSA (Sigma-Aldrich) was prepared at 1 mg/mL and dissolved in PBS. Ubiquitin, EGFP and HSP16.3 proteins were expressed using *E. coli*. Briefly, pRSET-bH6 plasmid carrying respective gene were transformed into BL21 and selected on ampicillin agar plate. A single colony was picked for expression using same protocol as described in 2.1. On the next day, the pellet was harvested and resuspended in lysis buffer (50 mM NaH_2PO_4, 300 mM NaCl, 10 mM imidazole, pH 7.4) with 20 µg/mL of lysozyme and incubated on ice for 1 h before proceeded to sonication. The cell suspension was then centrifuged at 10000 × *g* for 10 min at 12°C. The supernatant was loaded to 1 mL Ni-NTA agarose pre-equilibrated with binding buffer (20 mM NaH_2PO_4, 500 mM NaCl, 20 mM imidazole, pH 7.4). After 1 h incubation on rotator, the resin was washed with 20 mL of binding buffer and eluted at 1 mL fraction with elution buffer (20 mM NaH_2PO_4, 500 mM NaCl, 500 mM imidazole, pH 7.4). The protein concentration was determined using Bradford assay.

2.8 Luciferase reporter gene assay for interferon (IFN) promoter activation

scFv clones were subcloned to pcDNA3.1. Luciferase reporter gene assay was adapted from a protocol described previously [28, 29]. Briefly, HEK293T cells (1.5×10^4 cells/well) were seeded in 96 well plate 24 h before transfection. Cells were transfected using T-Pro P-Fect Transfection-III Reagent, according to the manufacturer's protocol. Plasmids were mixed with the transfection reagent in Opti-MEM I Reduced Serum Medium (Gibco) and incubated 15 min at RT. Transfection complexes were then gently added into individual wells of the 96 well plate. 24 h after transfection, cells were stimulated with IAV-RNA

(obtained as reported previously [30]) pre-mixed with the transfection reagent in Opti-MEM I Reduced Serum Medium, and incubated for 24 h at 37 °C in 5% CO_2. Cells were harvested with lysis buffer (50 mM Na-MES, 50 mM Tris-HCl, 1 mM dithiothreitol, 0.2% (v/v) Triton X-100, pH 7.8), and the lysates were added to luciferase assay buffer (125 mM Na-MES, 125 mM Tris-HCl, 25 mM magnesium acetate, 2.5 mg/mL ATP, pH 7.8). Immediately after addition of 50 µL of Luciferin buffer (25 mM D-luciferin, 5 mM KH_2PO_4), the luminescence was measured in Victor3 luminometer (Perkin Elmer). The luminescence was measured again after addition of 50 µL of Coelenterazine assay buffer (125 mM Na-MES, 125 mM Tris-HCl, 25 mM magnesium acetate, 5 mM KH_2PO_4 and 10 µM Coelenterazine, pH 7.8). The relative light units (RLU) of Luciferase signal were normalized to Renilla luciferase and over unstimulated controls. Each assay was performed in triplicate. Results were presented as folds of IFN promoter induction over the empty vector and plotted as mean and standard deviation of replicates with GraphPad Prism 6.01. Data were analysed with an unpaired two tailed t-test using a 95% confidence interval.

2.9 Epitope prediction of VP35

The epitopes of VP35 was predicted using BepiPred-2.0 [31], SVMTriP [32], CBTope [33], Discotope [34] and antibody epitope prediction under IEDB server [35-37]. The epitopes were identified via the consensus prediction results.

2.10 Structure prediction of scFv clones

The 3D structure of scFv clones were modelled using MODELLERv10.1 [38-41]. The built structures were then evaluated using QMEAN score in SWISS-MODEL server,

PROCHECK Ramachandran Plot [42, 43] and Verify3D [44, 45] to determine the ideal structure.

2.11 Docking of scFv clones (A2, A5 and G3) against VP35 protein

The scFv clones were docked against VP35 protein using HADDOCK server [46, 47] by restraining the docking region at the CDR regions of scFvs and the epitopes of VP35. The docked complex of scFv-VP35 was further assessed using jsPISA [48], PRODIGY [49, 50] and MM/GBSA calculation in HawkDock [51-54].

2.12 Molecular dynamics (MD) simulation of scFv-VP35 complex

The dynamics of scFv in complexed with VP35 were further studied using MD simulation. The ff14SB force field [55] in AMBER18 [56] via CUDA-enabled Particle Mesh Ewald Molecular Dynamics (PMEMD.cuda) were applied. Chloride ions were added to neutralize the charges of the system. The scFv-VP35 complex was solvated with at least 10 Å octahedral TIP3P water model from each direction. The complex was minimized with 4000 steps steepest descent minimization followed with 4000 steps conjugate gradient minimization. The distance of non-bonded interaction was set at 10 Å cut off. Next, the complex was heated to 300 K in 100 ps with SHAKE constraint. The complex was then equilibrated with 2 kcal/mol/Å2 restraint for 100 ps, followed by constant pressure equilibration for 15 ns. A total of 300 ns MD simulation with 0.1 ns interval for each frame was conducted. The final 10 ns of the simulation with 100 ps interval was used for free binding energy (ΔG) calculation, computational alanine scanning and pairwise energy decomposition using molecular mechanic Poisson Boltzmann (MMGBSA)/ Generalized Born (MMPBSA) surface area calculations [57]. In computational alanine scanning, the difference

in free binding energy (ΔΔG) after alanine mutation was calculated as deduction of free binding energy after alanine mutation from free binding energy of wild type complex. Hotspot residue was defined as residue in CDR with ΔG or ΔΔG ≤ -1 kcal/mol in both MMGBSA and MMPBSA calculations. The analysis was performed using UCSF Chimera version 1.15 [58]. The figures were prepared using PyMol [59].

3. Results

3.1 Identification of human monoclonal antibody against EBOV rVP35

VP35 protein of EBOV was expressed in *E. coli* and purified as described previously [23] with some modification. Purified recombinant VP35 (rVP35) was analysed on 12% SDS-PAGE and verified using western blot before proceeding to biopanning. A specific band at approximately 40 kDa was observed in Coomassie Blue-stained gel and the same band was detected by anti-His antibody in western blot indicating the EBOV rVP35 protein was successfully expressed (Fig. S1).

In order to obtain phage-displayed monoclonal antibodies binding to rVP35 protein, an existing in-house naïve scFv Human AntibodY LibrarY (HAYLY ver 2.0) with a diverse repertoire was used [24]. The scFv population against rVP35 was enriched over two rounds of biopanning and polyclonal ELISA demonstrated in Fig. 1 (a) showed increment of the absorbance reading at 405nm (OD_{405nm}) from 0.103 to 1.431 with low background signal of 0.084 and 0.096 for round 1 and 2, respectively. The signal over noise ratio (S/N) is 1.226 and 14.906 for round 1 and 2 respectively, indicating successful enrichment of rVP35 binders over 2 panning rounds.

Subsequent to polyclonal ELISA, round 2 phage was serial diluted and plated out for monoclonal selection. 92 colonies were picked randomly, and several hits were obtained as shown in Fig. 1 (b). The absorbance reading of the sample (coated with rVP35) were divided with the background reading (coated with BSA) and was presented as S/N ratio in a heatmap. Clones with higher S/N ratio after 30 min incubation were identified for further evaluation as prospective leads. In total, there were 36 clones that demonstrated a S/N above 2 and these clones were further examined with colony PCR to ensure full scFv inserts were present (Fig. S2). Based on the colony PCR, all clones showed a band size of approximately 1200 base pair (bp), which corresponds to the band size of a full scFv insert. Finally, a total of ten colonies with the highest readings in monoclonal ELISA (A2, A5, B2, D1, E10, E11, E12, G1, G3, H9) were sequenced. The sequencing results showed several clones having identical sequences which is common due to the enrichment of clones from the panning rounds. The sequences were grouped to identify three unique clones, namely A2, A5 and G3. The V(D)J genes of each clone were analysed in IMGT/V-QUEST [25, 26] and a summary of the results are demonstrated in Table 1. Both clone A2 and A5 have the same V-gene families which is IGHV3 with differences in D- and J-gene of heavy chain. Clone A2 sequence shows the use of IGHD2-8 and IGHJ5 whereas clone A5 used IGHD3-22 and IGHJ2. The light chain for both clone A2 and A5 were similar with IGKV2 and IGKJ2 being used. Clone G3 was unique with a V(D)J combination of IGHV4, IGHD3-10 and IGHJ6 being used together with IGLV3 and IGLJ2,

3.2 Characterization of soluble anti-VP35 scFv clone expression

We also wanted to investigate the role of sequence variation on soluble scFv expression in different host systems. In this case, we wanted to see if the expression of

soluble scFv would be comparable between standard *E. coli* and *L. tarentolae* expression systems. The scFv clones were transformed into *E. coli* HB2151 and SHuffle T7 using standard procedures as a standard control. The clones were first expressed in *E. coli* HB2151, but only clone G3 was expressed and successfully extracted from the periplasmic fraction (Fig. S3 (a)). Clone A2 and A5 were transformed to *E. coli* SHuffle T7 and majority of the protein were found in the pellet even after periplasmic and cytoplasmic extraction (Fig. S3 (b)). Hence the proteins were extracted using 8 M urea buffer. The extracted protein of all three clones were later subjected to immobilized metal affinity chromatography (IMAC) purification using the same protocol which utilizes phosphate buffer with imidazole. As shown in Fig. 2 (a) and (b), a band size of approximately 35 kDa was visible indicating the three scFv clones were expressed, extracted, and purified from *E. coli*. The same anti-VP35 clones were subcloned to pLTEX-5.2 for expression in *L. tarentolae*. Plasmid pLTEX-5.2 was modified from pLTEX-5 [27] to harbour a myc-tag fusion to the scFv for downstream detection as the clones A2 and A5 from light chain family IGKV2 were not able to be detected by Protein L HRP. Fig. 2 (c) showed the Coomassie Blue-stained SDS-PAGE of clone A2 and G3 purified using Ni-NTA resin. Interestingly, clone A5 could not be expressed in *L. tarentolae* after several attempts showing a potential influence of sequence bias between the expression tolerance of the two hosts. However, clones A2 and G3 were expressed well on *L. tarentolae.*

Binding of the anti-VP35 clones expressed in *E. coli* and *L. tarentolae* to rVP35 were tested. Fig. 3 (a) showed A2 and A5 expressed from *E. coli* have stronger binding signal compared to G3. The specificity of the clones was tested by coating other proteins such as BSA, ubiquitin, enhanced green fluorescent protein (EGFP) and HSP16.3 as target and the results showed the scFv clones were all binding specifically to the rVP35 only. Titration curves of different amount of scFv (10 μg, 5 μg, 2.5 μg, 1.25 μg, 0.625 μg and 0 μg) against

fixed amount of rVP35 (1 μg) were assayed (Fig. 3 (b)). All the clones showed direct correlation between the increase of the binding signal and the amount of scFv. A similar trend was observed when the clones expressed *in L. tarentolae* were used for titration curve, where A2 showed a slightly higher signal compared to G3 (Fig. 3 (c)).

3.3 Assessment on the inhibitory effect of anti-VP35 scFv clones to VP35 *in vitro*

It is known that EBOV VP35 impairs the host's innate immune system by blocking the production of IFN. To study the ability of A2, A5 and G3 in reverting the IFN antagonistic function of VP35, a luciferase reporter gene assay was carried out as described previously [5]. The scFv genes were subcloned to pcDNA3.1 and co-transfected with pcDNA3-VP35 to HEK293T cells which were stimulated with IAV-RNA later to activate the IFN-β promoter for concurrent production of IFN and luciferase. The lysates of harvested cells were then tested in luciferase assay where the induction of IFN-β promoter was implicated in relative light units (RLU) of luciferase signal. The result is demonstrated in Fig. 4 as folds of IFN promoter induction over empty vector.

All 3 clones showed for most of the conditions tested a statistically significant level of inhibition on VP35 (Table S1) as higher fold of IFN promoter induction was detected as compared to the control transfected with VP35 plasmid only. However, the expression of the IFN was not restored fully as demonstrated in the control without VP35. The inhibition did not show a consistent trend when the amount of scFv plasmid transfected was increased.

3.4 Molecular Docking of anti-VP35 A2 to VP35

VP35 interferes the IFN production through the interferon inhibitory domain (IID). Thus, prediction of the potential epitope was conducted on the C-terminal IID of VP35 protein between residues 215 to 340. The analysis (Table 2) has suggested that there were 29 residues as possible epitopes along VP35 C-terminal IID. Literatures showed that residues 298-322 and 329-338 [60, 61] as well as residue 339 [61] are involved in the interactions with dsRNA when blocking expression of IFN. Thus, residues 298-322 and 329-339 were used as the active regions in the docking with scFv clones.

Then, the 3D structure of scFvs tertiary structure was built and assessed in term of the model compatibility to its sequence (Verify3D), quality estimation on the geometrical analysis (QMEAN) and the statistical distribution of the model's backbone ϕ and ψ angles (Ramachandran plot). Analysis showed that the predictive structure of A2, A5 and G3 are in good quality. A2 has Verify3D profile score of 98.55%, QMEAN score of 0.7 and 91.2% of residues in the most favoured regions of the Ramachandran plot. A5 also showed high Verify3D profile score (97.78%), 0.69 of QMEAN score and 88% of residues in the most favoured regions on the Ramachandran plot. The structure of G3 scFv contains 85.2% of residues in the most favoured regions on the Ramachandran plot, QMEAN score of 0.62 and 94.44% Verify3D profile score. All three models of scFvs contain 0.5% of residue located in the disallowed regions of the Ramachandran plot, which is equivalent to one residue in each modelled scFv. The residue in disallowed region of A2, A5 and G3 was A213, V120 and S62, respectively. However, these residues were not a major concern as they are not located in the scFv CDR regions which are responsible for the interaction with VP35.

Subsequent to VP35 epitope prediction and anti-VP35 scFvs structural modelling, docking study was carried out. The docked conformations of scFv-VP35 were evaluated based on the binding free energy (ΔG), interface area and dissociation constant (Kd). Results

indicated that A2, A5 and G3 are favourable to bind with VP35 with their binding free energies, large interfacial areas and low Kd values (Table S2).

3.5 Molecular dynamics (MD) simulation of scFv-VP35 complex

A total of 300 ns molecular dynamics simulation was conducted on three scFv-VP35 complexes namely A2-VP35, A5-VP35 and G3-VP35. All scFv-VP35 complexes showed stable RMSD and RMSF throughout the simulations (Fig. S4). MMGBSA and MMPBSA binding free energy calculations using the last 10 ns of the simulation revealed that A2 interacted VP35 with ΔG of -10.58 ± 5.28 kcal/mol and -32.34 ± 7.66 kcal/mol, respectively, while G3-VP35 complex was ΔG of -12.33 ± 5.24 kcal/mol and -30.05 ± 7.37 kcal/mol, respectively (Table 3). However, A5-VP35 showed a higher ΔG of -51.99 ± 8.37 kcal/mol and -51.34 ± 10.04 kcal/mol according to MMGBSA and MMPBSA calculations. The MMGBSA and MMPBSA analysis also suggested that the interactions between A2 and VP35 were mainly driven by favourable van der Waals energy. The van der Waals interactions between A2-VP35 complex would have antagonized the unfavourable electrostatic interactions resulting in an overall favourable ΔG. In contrast, A5 and G3 showed higher favourable electrostatic interactions with VP35, although they required higher solvation energy.

3.6 CDRs analysis for anti-VP35 A2

Due to the better *in vitro* binding activity of A2 with VP35 protein compared to the other scFvs, computational alanine scanning (CAS) was conducted using A2-VP35 complex as a reference in compared to other scFvs. CAS analysis suggested that among the CDRs, A2 heavy chain CDR3 and light chain CDR1 contributed the most to the favourable binding with

VP35. A2 heavy chain CDR3 and light chain CDR1 exhibited $\Delta\Delta G_{Total}$ -6.64 and -6.42 kcal/mol, respectively, in MMGBSA calculation, while MMPBSA calculation showed $\Delta\Delta G_{Total}$ of -2.36 and -4.72 kcal/mol for A2 heavy chain CDR3 and light chain CDR1, respectively (Table 4). Amongst the residues in A2 heavy chain CDR3, Y106 was the principal contributor to $\Delta\Delta G_{Total}$ with -6.56 and -2.13 kcal/mol from MMGBSA and MMPBSA, respectively. While H184 and Y190 are the most important residues in A2 light chain CDR1, MMGBSA and MMPBSA estimated H184 $\Delta\Delta G_{Total}$ of -2.78 and -2.17 kcal/mol, respectively, whereas Y190 $\Delta\Delta G_{Total}$ of -3.4 and -1.99 kcal/mol, respectively.

From the pairwise decomposition analysis, A2 heavy chain CDR2 demonstrated the most negative ΔG_{Total} of -24.57 and -18.47 kcal/mol in MMGBSA and MMPBSA calculations, respectively (Table 5). This was followed by A2 light chain CDR3 with -14.25 and -12.84 kcal/mol for MMGBSA and MMPBSA calculations, respectively. The A2 heavy chain CDR3 and light chain CDR1 were also showing favourable ΔG_{Total}, although less favourable than CDR2 of heavy chain and CDR3 of light chain in the scFv. Their respective ΔG_{Total} were -10.44 and -10.96 kcal/mol for MMGBSA calculation, and -6.33 and -9.79 kcal/mol for MMPBSA calculation.

The average A2 VP35 conformation from the last 10 ns of MD simulation was depicted in Fig. 5 (a). Within heavy chain CDR2, four hotspot residues were exhibited ΔG_{Total} < -1 kcal/mol in both MMGBSA and MMPBSA calculations (Fig. 5 (b)). Y56 showed the lowest ΔG_{Total}, followed by G58, G57 and T60 in MMGBSA calculation with the respective ΔG_{Total} of -8.89, -6.24, -3.97 and -1.37 kcal/mol. Similar trend was found using MMPBSA calculation with ΔG_{Total} of -6.54, -4.91, -3.57 and -2.21 kcal/mol, respectively. Three hotspot residues were found in light chain CDR3 (Fig. 5 (c)). L250 shows the most negative ΔG_{Total} of -6.62 and -6.46 kcal/mol in MMGBSA and MMPBSA calculations, respectively. The other two hotspot residues, Q251 and T252 have the respective ΔG_{Total} of -4.03 and -2.51 kcal/mol

using MMGBSA calculation and, -3.23 and -1.26 kcal/mol using MMPBSA calculation. H184 and Y190 were the hotspot residues in light chain CDR1 whereas only one hotspot residue (Y106) was found in heavy chain CDR3. MMGBSA estimated ΔG_{Total} of H184 and Y190 were -4.41 and -4.66 kcal/mol, respectively. MMPBSA indicated comparable ΔG_{Total} of -2.77 and -5.06 kcal/mol for H184 and Y190, respectively. ΔG_{Total} in heavy chain CDR3 mainly contributed by Y106 with ΔG_{Total} of -9.42 and -6.13 kcal/mol in MMGBSA and MMPBSA calculations, respectively.

Compared to A2, all CDR except for CDR2 in A5 light chain interacted with VP35. An interaction was noticed between A5 heavy chain CDR1 and VP35 with ΔG_{Total} of -24.62 kcal/mol and -24.03 kcal/mol from MMGBSA and MMPBSA calculations, respectively (Table 5). The pairwise decomposition analysis suggested that A5 heavy chain CDR1 S30, R31 and D33 have a ΔG_{Total} of -2.91 kcal/mol, -3.88 kcal/mol and -17.46 kcal/mol, respectively based on MMGBSA calculations. MMPBSA calculation estimated that the ΔG_{Total} of these residues were -1.79 kcal/mol, -1.84 kcal/mol and -19.83 kcal/mol, respectively.

Besides, pairwise decomposition also suggested that the interactions of A5 heavy and light chain CDR3 with VP35 were stronger with -34.71 kcal/mol and -20.67 kcal/mol, respectively from MMGBSA calculation. A similar data was observed via MMPBSA calculations, where the ΔG_{Total} of A5 heavy and light chain CDR3 were -36.46 kcal/mol and -19.46 kcal/mol, respectively. E98, V100, D101, E103 and H108 were among the hotspot residues in A5 heavy chain CDR3 with ΔG_{Total} -15.71 kcal/mol, -5.14 kcal/mol, -3.03 kcal/mol, -3.5 kcal/mol and -4.93 kcal/mol, respectively from MMGBSA analysis. The MMPBSA calculation indicated that the hotspot residues have ΔG_{Total} of -21.47 kcal/mol, -2.52 kcal/mol, -4.04 kcal/mol, -3.71 kcal/mol and -3.66 kcal/mol, respectively. However, MMGBSA and MMPBSA calculations indicated that A5 heavy chain CDR3 Y102 has a

lower ΔG_{Total} of -0.57 kcal/mol and -0.3 kcal/mol, respectively, compared to A2 heavy chain CDR3 Y106.

Similarly, A5 light chain CDR3 L246, E247 and T248 are favourable with VP35 with ΔG_{Total} -1.07 kcal/mol, -11.86 kcal/mol and -7.33 kcal/mol, respectively from MMGBSA calculation. MMPBSA calculation estimated the ΔG_{Total} for these hotspot residues, which were -0.98 kcal/mol, -10.83 kcal/mol and -6.93 kcal/mol, respectively. Although most of A5 heavy and light chains CDR showed an increase in ΔG_{Total} when interacting with VP35 in comparison with the same region in A2 scFv, with the heavy chain CDR2 and light chain CDR1 giving decreased interactions with VP35 with only -16.43 kcal/mol of ΔG_{Total} from MMGBSA calculation. The respective ΔG_{Total} in this region were -1.47 kcal/mol (G52), -3.54 kcal/mol (T53), -1.64 kcal/mol (G54) and -8.72 kcal/mol (D56). The MMPBSA calculated ΔG_{Total} for these hotspot residues were -1.64 kcal/mol, -1.96 kcal/mol, -1.38 kcal/mol and -8.03 kcal/mol, respectively, which contributed to the major interactions in A5 heavy chain CDR2 with ΔG_{Total} -14.88 kcal/mol. Likewise, A5 light chain CDR1 has a lower ΔG_{Total} compared to A2 with -9.69 kcal/mol and -8.3 kcal/mol from MMGBSA and MMPBSA calculations, respectively. From MMGBSA and MMPBSA calculations, the hotspot residue in this region is D182 (ΔG_{Total} -6.91 kcal/mol and -7.45 kcal/mol, respectively). However, H180 and Y186 have only ΔG_{Total} -0.56 kcal/mol and -0.31 kcal/mol from MMPBSA calculation.

In G3 scFv, the CDR regions that interacted with VP35 protein were lesser than the other scFvs. Only CDR1 and CDR3 of the heavy chain, and CDR2 of light chain have ΔG_{Total} lower than -1 kcal/mol and their respective MMGBSA and MMPBSA calculated ΔG_{Total} were -8.9 kcal/mol and -8.23 kcal/mol for heavy chain CDR1, -34.17 kcal/mol and -28.47 kcal/mol for heavy chain CDR3, and -8.35 kcal/mol and -9.63 kcal/mol for light chain CDR2. Based on the MMGBSA and MMPBSA calculation of pairwise decomposition in CDR 1 of G3

heavy chain, the hotspot residues were S30 (ΔG_{Total} -1 kcal/mol and -1.36 kcal/mol, respectively), G31 (ΔG_{Total} -1.76 kcal/mol and -1.25 kcal/mol, respectively), Y32 (ΔG_{Total} -2.02 kcal/mol and -1.31 kcal/mol, respectively) and Y33 (ΔG_{Total} -3.22 kcal/mol and -2.4 kcal/mol, respectively). Whereas for G3 heavy chain CDR3, MMGBSA estimated that the hotspot residues Q100, V102, Y103, Y104 and Y105 have ΔG_{Total} of -7.78 kcal/mol, -2.89 kcal/mol, -5.31 kcal/mol, -8.11 kcal/mol and -8.53 kcal/mol, respectively. Similarly, MMPBSA calculated ΔG_{Total} in these hotspot residues were -6.49 kcal/mol, -2.58 kcal/mol, -6.46 kcal/mol, -5.31 kcal/mol, -6.09 kcal/mol and -1.3 kcal/mol, respectively. Compared to A2 and A5, G3 light chain CDR2 were distinct and this interaction with VP35 protein was only formed with G3. This could be due to D198 that contributed ΔG_{Total} -6.38 kcal/mol and -7.89 kcal/mol according to MMGBSA and MMPBSA calculations, respectively. In addition, A197 has also contributed ΔG_{Total} -1.64 kcal/mol and -1.89 kcal/mol with VP35 based on MMGBSA and MMPBSA calculations, respectively.

A comparison of the scFv residues in CDR regions has been performed in order to further study the interactions between the scFvs with VP35. Analysis suggested that there were numerous identical residues between the isolated scFvs (Table 6). In particular, the hotspot residues were identical between A2 and A5 with only Y56T mutation in A5 heavy chain CDR2 and A5 light chain CDR3 Q251E. On the other hand, G3 has no identical residues in the light chain compared to A2, but the heavy chain still resembled A2 with only Y56Q and G57S mutation in G3 heavy chain CDR2. Additionally, the identical hotspot residues found in both A5 and G3 scFvs were also structurally located at the similar location as in A2 (Fig. 6)

4. Discussion

A large outbreak of EVD that persistent for three years in 2014 – 2016 has raised huge concern amongst healthcare institutions resulting in the quest to find more effective therapy and diagnostic measures for the management of EVD. In October and December of 2020, two monoclonal antibody therapies were approved by USFDA, namely and Inmazeb and Ebanga. Inmazeb is an antibody cocktail containing three monoclonal antibodies - atoltivimab, maftivimab, and odesivimab-ebgn, whereas Ebanga is a single monoclonal antibody [9]. Both therapies target the GP of EBOV. Although there are no mAbs against VP35 in the market, it is an interesting and promising target because of its role as an IFN antagonist. Interference of VP35 on IFN production hampers the host cell innate immune response to the virus. Additionally, efficient IFN production can be restored upon inhibition of VP35 IFN antagonism, bocking viral replication [29].

In this study, we have utilized human naïve scFv library to identify mAbs against EBOV VP35. A combinatorial naïve library with a repertoire diversity as large as 10^9 clones should, in theory be diverse enough to obtain antibody binders against any target [21]. Here we successfully obtained three unique clones from the naïve library, of which two of the clones, A2 and A5 are from gene family of IGHV3 and IGKV2, whereas another clone G3 is from IGHV4 and IGLV3 (Table 1). Although A2 and A5 show similarity in the heavy and light chain gene families combination, the CDRs are the unique regions responsible for the antibody-antigen interaction. This could explain the difference in the binding affinity of the A2, A5 and G3 on the *in vitro* ELISA assay.

The 3 unique clones were then expressed in soluble form using two different expression systems, *E. coli* and *L. tarentolae.* We wanted to see if the sequence variation between the clones would interfere with the expression outcomes in *E. coli* and *L. tarentolae.* The three clones were well expressed in *E. coli* but clone A5 was not expressed in *L. tarentolae.* Although clones A2 and A5 were of IGHV3 and IGKV2 family sequence, the

expression patterns in *L. tarentolae* were different. This could indicate the influence of the D and J segments on the expression profiles of antibody clones in *L. tarentolae.* A previous study showed the influence of secretary peptides on the expression of several scFv clones in *L. tarentolae* [27]. The study showed the suitability of pelB as a leader peptide for expression. However, the clones used were of a similar framework based on an optimized semi-synthetic antibody scaffold for expression. Although *L. tarentolae* is touted as a potential alternative expression host for scFv expression [27], the conditions and parameters for antibody expression in *L. tarentolae* with diverse framework sequences would require further understanding. Even so, the data indicating that the three clones were binding to the target by phage and *E. coli* was sufficient to investigate the 3 clones for functionality.

In the luciferase reporter gene assay, the three clones showed a significant inhibition of VP35 interferon antagonism function, as demonstrated on the signal of luciferase which implicates activation of IFN promoter for co-expression of luciferase and IFN. Although the ELISA showed binding of the clones to rVP35, the inhibition effect in cell assay was not high. It could either be because of the scFvs are binding to region outside of the VP35 IID or the expression of the antibodies were not optimum in intracellular setting. Since the clones originated from a naïve combinatorial library, the sequence combination might affect the efficiency of protein transcription and translation. In fact, the expression level of a recombinant protein, as well as the protein structure and folding are influenced greatly by the codon usage bias of the expression host [62, 63]. As demonstrated in the two expression systems utilized in this study, the expression result for A5 was significantly different when using *E. coli* compared to *L. tarentolae*. A5 was not able to express in *L. tarentolae* but was produced in higher amounts in *E. coli*. The scFvs expressed in *L. tarentolae* were analysed on non-reducing SDS-PAGE and the band pattern is different from the control scFv expressed using *E. coli*. This might indicate potential post-translational modification on the scFv. The

possible post-translational modification might also affect the binding *in vivo* as a result of structural changes [64]. However, clone A2 showed the most promising inhibition pattern of the three clones. Therefore, clone A2 was further evaluated structurally to predict the interaction patterns of the clone.

The interaction of the clone A2 with EBOV VP35 was modelled computationally. The docking of A2 on VP35 C-terminal IID domain indicated favourable binding affinity. Structural analysis from A2-VP35 MD simulation suggested that the complex was relatively stable throughout the simulation as indicated in the RMSD and RMSF. Binding free energy calculation using MMGBSA and MMPBSA approaches further evidenced the interaction between A2 and VP35 driven mainly by favourable van der Waals interactions. Both computational alanine scanning and pairwise decomposition obtained from A2-VP35 MD simulation trajectories suggested that A2 Y106 in heavy chain CDR3, H184 and Y190 in light chain CDR1 are among the hotspot residues in the interactions with VP35. Pairwise decomposition analysis also showed that A2 heavy chain CDR2 and light chain CDR3 were contributed to ΔG compared with heavy chain CDR3 and light chain CDR1. A2 Y56, G58, G57 and T60 in heavy chain CDR2 and, L250, Q251 and T252 in light chain CDR3 were the hotspot residues involving in interacting with VP35.

Likewise, residues comparison in CDRs of all three scFv clones suggested that the identified hotspot residues were playing an important role in interacting with VP35. The conserved hotspot residues among the three scFv clones also indicated that all scFv clone might interact in a similar manner to VP35.

There are several limitations to our current study. One of the main limitations is the ability of the clones to function intracellularly which could be overcome by engineering [65]. Additionally, the absence of performing the assay using actual viruses is something that could

be addressed in the future. Even so, the mAbs isolated could also be develop as a diagnostic tool in addition to the therapeutic potential. EVD being a highly contagious disease that spread through direct contact of body fluid. Therefore, early detection and quick response to contain infected individuals are critical to break the transmission chain. Current diagnostics are carried out using RT-PCR and antigen tests using mAbs from immunized mice for detection of viral GP, NP, and VP40 which are essentially the shell of the EBOV. Considering the setting of EVD outbreaks are often concentrated at rural areas of Africa where access to RT-PCR is limited and time-consuming, rapid point-of-care detection using antigen-antibody capture such as lateral flow assay could be more advantageous for rapid diagnosis for EVD.

5. Conclusion

In brief, three scFv clones against EBOV VP35 originated from human naïve phage-displayed library were identified. The clones showed binding affinities in ELISA, the luciferase reporter gene assay only showed certain level of inhibition on VP35. Computational modelling has suggested favourable interaction of the clones with VP35 IID, further studies could be conducted to optimize the clone for better binding extra- and intracellularly. It is likely that the clones would have to undergo further affinity engineering or format conversion for improved inhibition activity.

CRediT authorship contribution statement

Jing Yi Lai: Methodology, Investigation, Formal analysis, Writing – Original Draft, Visualization. **Angela Corona**: Methodology, Investigation, Formal analysis, Writing – Original Draft, Writing – Review & Editing, Visualization. **Chong Lee Ng**: Methodology,

Investigation, Formal analysis, Writing – Original Draft, Visualization. **Enzo Tramontano**: Conceptualization, Supervision, Writing – Review & Editing. **Yee Siew Choong**: Conceptualization, Supervision, Writing – Review & Editing. **Theam Soon Lim**: Conceptualization, Methodology, Supervision, Funding acquisition, Writing – Original Draft, Writing – Review & Editing.

Declaration of competing interest

The authors declare no competing financial interest.

Acknowledgement

The authors would like to acknowledge financial support from Universiti Sains Malaysia Special (Matching) Short-Term Grant with Project No: 304.CIPPM.6315708.

References

[1] C. Report of an International, Ebola haemorrhagic fever in zaire, 1976, Bulletin of the World Health Organization 56(2) (1978) 271-293.
[2] J.H. Kuhn, Y. Bào, S. Bavari, S. Becker, S. Bradfute, K. Brauburger, J. Rodney Brister, A.A. Bukreyev, Y. Caì, K. Chandran, R.A. Davey, O. Dolnik, J.M. Dye, S. Enterlein, J.-P. Gonzalez, P. Formenty, A.N. Freiberg, L.E. Hensley, T. Hoenen, A.N. Honko, G.M. Ignatyev, P.B. Jahrling, K.M. Johnson, H.-D. Klenk, G. Kobinger, M.G. Lackemeyer, E.M. Leroy, M.S. Lever, E. Mühlberger, S.V. Netesov, G.G. Olinger, G. Palacios, J.L. Patterson, J.T. Paweska, L. Pitt, S.R. Radoshitzky, E.I. Ryabchikova, E.O. Saphire, A.M. Shestopalov, S.J. Smither, N.J. Sullivan, R. Swanepoel, A. Takada, J.S. Towner, G. van der Groen, V.E. Volchkov, V.A. Volchkova, V. Wahl-Jensen, T.K. Warren, K.L. Warfield, M. Weidmann, S.T. Nichol, Virus nomenclature below the species level: A standardized nomenclature for filovirus strains and variants rescued from cdna, Archives of Virology 159(5) (2014) 1229-1237.
[3] T. Goldstein, S.J. Anthony, A. Gbakima, B.H. Bird, J. Bangura, A. Tremeau-Bravard, M.N. Belaganahalli, H.L. Wells, J.K. Dhanota, E. Liang, The discovery of bombali virus adds further support for bats as hosts of ebolaviruses, Nature microbiology 3(10) (2018) 1084-1089.
[4] L. Baseler, D.S. Chertow, K.M. Johnson, H. Feldmann, D.M. Morens, The pathogenesis of ebola virus disease, Annual Review of Pathology: Mechanisms of Disease 12(1) (2017) 387-418.
[5] M.-A. Conteh, S.T. Goldstein, H.R. Wurie, J. Gidudu, D.R. Lisk, R.J. Carter, J.F. Seward, L.M. Hampton, D. Wang, L.E. Andersen, M. Arvay, S.J. Schrag, P. Lawson, A.E. Fombah, C.R. Petrie, D.R. Feikin, J.B.W. Russell, R. Lindblad, S.A.S. Kargbo, M. Sesay, B.E. Mahon, Clinical surveillance and evaluation of suspected ebola cases in a vaccine trial during an ebola epidemic: The sierra leone trial to introduce a vaccine against ebola, The Journal of Infectious Diseases 217(suppl_1) (2018) S33-S39.
[6] A.M. Henao-Restrepo, A. Camacho, I.M. Longini, C.H. Watson, W.J. Edmunds, M. Egger, M.W. Carroll, N.E. Dean, I. Diatta, M. Doumbia, B. Draguez, S. Duraffour, G. Enwere, R. Grais, S. Gunther, P.-S. Gsell, S. Hossmann, S.V. Watle, M.K. Kondé, S. Kéïta, S. Kone, E. Kuisma, M.M. Levine, S. Mandal, T. Mauget, G. Norheim, X. Riveros, A. Soumah, S. Trelle, A.S. Vicari, J.-A. Røttingen, M.-P. Kieny, Efficacy and effectiveness of an rvsv-vectored vaccine in preventing ebola virus disease: Final results from the guinea ring vaccination, open-label, cluster-randomised trial (ebola ça suffit!), The Lancet 389(10068) (2017) 505-518.
[7] S. Mulangu, L.E. Dodd, R.T. Davey, O. Tshiani Mbaya, M. Proschan, D. Mukadi, M. Lusakibanza Manzo, D. Nzolo, A. Tshomba Oloma, A. Ibanda, R. Ali, S. Coulibaly, A.C. Levine, R. Grais, J. Diaz, H.C. Lane, J.-J. Muyembe-Tamfum, P.W.G. the, A randomized, controlled trial of ebola virus disease therapeutics, New England Journal of Medicine 381(24) (2019) 2293-2303.
[8] V. Wahl-Jensen, S. Kurz, T. Feldmann, L.K. Buehler, J. Kindrachuk, V. DeFilippis, J. da Silva Correia, K. Früh, J.H. Kuhn, D.R. Burton, Ebola virion attachment and entry into human macrophages profoundly effects early cellular gene expression, PLoS neglected tropical diseases 5(10) (2011) e1359.
[9] M.M. Levine, Monoclonal antibody therapy for ebola virus disease, New England Journal of Medicine 381(24) (2019) 2365-2366.
[10] T. Shu, T. Gan, P. Bai, X. Wang, Q. Qian, H. Zhou, Q. Cheng, Y. Qiu, L. Yin, J. Zhong, X. Zhou, Ebola virus vp35 has novel ntpase and helicase-like activities, Nucleic acids research 47(11) (2019) 5837-5851.
[11] Y. Takamatsu, L. Kolesnikova, S. Becker, Ebola virus proteins np, vp35, and vp24 are essential and sufficient to mediate nucleocapsid transport, Proc Natl Acad Sci U S A 115(5) (2018) 1075-1080.
[12] D.W. Leung, K.C. Prins, C.F. Basler, G.K. Amarasinghe, Ebolavirus vp35 is a multifunctional virulence factor, Virulence 1(6) (2010) 526-531.
[13] K.C. Prins, S. Delpeut, D.W. Leung, O. Reynard, V.A. Volchkova, S.P. Reid, P. Ramanan, W.B. Cárdenas, G.K. Amarasinghe, V.E. Volchkov, C.F. Basler, Mutations abrogating vp35 interaction with double-stranded rna render ebola virus avirulent in guinea pigs, J Virol 84(6) (2010) 3004-3015.

[14] E. Fanunza, A. Frau, A. Corona, E. Tramontano, Insights into ebola virus vp35 and vp24 interferon inhibitory functions and their initial exploitation as drug targets, Infect Disord Drug Targets 19(4) (2019) 362-374.
[15] C. Woolsey, A.R. Menicucci, R.W. Cross, P. Luthra, K.N. Agans, V. Borisevich, J.B. Geisbert, C.E. Mire, K.A. Fenton, A. Jankeel, S. Anand, H. Ebihara, T.W. Geisbert, I. Messaoudi, C.F. Basler, A vp35 mutant ebola virus lacks virulence but can elicit protective immunity to wild-type virus challenge, Cell Rep 28(12) (2019) 3032-3046.e3036.
[16] W. Seesuay, S. Jittavisutthikul, N. Sae-lim, N. Sookrung, Y. Sakolvaree, W. Chaicumpa, Human transbodies that interfere with the functions of ebola virus vp35 protein in genome replication and transcription and innate immune antagonism, Emerging Microbes & Infections 7(1) (2018) 1-15.
[17] M. Flego, A. Frau, L. Accardi, A. Mallano, A. Ascione, M. Gellini, E. Fanunza, S. Vella, P. Di Bonito, E. Tramontano, Intracellular human antibody fragments recognizing the vp35 protein of zaire ebola filovirus inhibit the protein activity, BMC Biotechnol 19(1) (2019) 64.
[18] K.E. Pascal, D. Dudgeon, J.C. Trefry, M. Anantpadma, Y. Sakurai, C.D. Murin, H.L. Turner, J. Fairhurst, M. Torres, A. Rafique, Y. Yan, A. Badithe, K. Yu, T. Potocky, S.L. Bixler, T.B. Chance, W.D. Pratt, F.D. Rossi, J.D. Shamblin, S.E. Wollen, J.M. Zelko, R. Carrion, Jr., G. Worwa, H.M. Staples, D. Burakov, R. Babb, G. Chen, J. Martin, T.T. Huang, K. Erlandson, M.S. Willis, K. Armstrong, T.M. Dreier, A.B. Ward, R.A. Davey, M.L.M. Pitt, L. Lipsich, P. Mason, W. Olson, N. Stahl, C.A. Kyratsous, Development of clinical-stage human monoclonal antibodies that treat advanced ebola virus disease in nonhuman primates, The Journal of Infectious Diseases 218(suppl_5) (2018) S612-S626.
[19] D. Corti, J. Misasi, S. Mulangu, D.A. Stanley, M. Kanekiyo, S. Wollen, A. Ploquin, N.A. Doria-Rose, R.P. Staupe, M. Bailey, W. Shi, M. Choe, H. Marcus, E.A. Thompson, A. Cagigi, C. Silacci, B. Fernandez-Rodriguez, L. Perez, F. Sallusto, F. Vanzetta, G. Agatic, E. Cameroni, N. Kisalu, I. Gordon, J.E. Ledgerwood, J.R. Mascola, B.S. Graham, J.-J. Muyembe-Tamfun, J.C. Trefry, A. Lanzavecchia, N.J. Sullivan, Protective monotherapy against lethal ebola virus infection by a potently neutralizing antibody, Science 351(6279) (2016) 1339-1342.
[20] M.A. Alfaleh, H.O. Alsaab, A.B. Mahmoud, A.A. Alkayyal, M.L. Jones, S.M. Mahler, A.M. Hashem, Phage display derived monoclonal antibodies: From bench to bedside, Frontiers in Immunology 11 (2020).
[21] S.K. Chan, A. Rahumatullah, J.T. Lai, T.S. Lim, Naïve human antibody libraries for infectious diseases, in: T.S. Lim (Ed.), Recombinant antibodies for infectious diseases, Springer International Publishing, Cham, 2017, pp. 35-55.
[22] K.T. Xenaki, S. Oliveira, P.M.P. van Bergen en Henegouwen, Antibody or antibody fragments: Implications for molecular imaging and targeted therapy of solid tumors, Frontiers in Immunology 8 (2017).
[23] L. Zinzula, F. Esposito, E. Mühlberger, M. Trunschke, D. Conrad, D. Piano, E. Tramontano, Purification and functional characterization of the full length recombinant ebola virus vp35 protein expressed in e. Coli, Protein Expression and Purification 66(1) (2009) 113-119.
[24] B.N. Lim, C.F. Chin, Y.S. Choong, A. Ismail, T.S. Lim, Generation of a naïve human single chain variable fragment (scfv) library for the identification of monoclonal scfv against salmonella typhi hemolysin e antigen, Toxicon 117 (2016) 94-101.
[25] V. Giudicelli, X. Brochet, M.P. Lefranc, Imgt/v-quest: Imgt standardized analysis of the immunoglobulin (ig) and t cell receptor (tr) nucleotide sequences, Cold Spring Harbor protocols 2011(6) (2011) 695-715.
[26] X. Brochet, M.P. Lefranc, V. Giudicelli, Imgt/v-quest: The highly customized and integrated system for ig and tr standardized v-j and v-d-j sequence analysis, Nucleic acids research 36(Web Server issue) (2008) W503-508.
[27] S. Klatt, Z. Konthur, Secretory signal peptide modification for optimized antibody-fragment expression-secretion in leishmania tarentolae, Microbial Cell Factories 11(1) (2012) 97.

[28] E. Fanunza, M. Iampietro, S. Distinto, A. Corona, M. Quartu, E. Maccioni, B. Horvat, E. Tramontano, Quercetin blocks ebola virus infection by counteracting the vp24 interferon-inhibitory function, Antimicrobial agents and chemotherapy 64(7) (2020).
[29] A. Corona, E. Fanunza, C. Salata, M.J. Morwitzer, S. Distinto, L. Zinzula, C. Sanna, A. Frau, G.L. Daino, M. Quartu, O. Taglialatela-Scafati, D. Rigano, S. Reid, A. Mirazimi, E. Tramontano, Cynarin blocks ebola virus replication by counteracting vp35 inhibition of interferon-beta production, Antiviral Research 198 (2022) 105251.
[30] V. Cannas, G.L. Daino, A. Corona, F. Esposito, E. Tramontano, A luciferase reporter gene assay to measure ebola virus viral protein 35–associated inhibition of double-stranded rna–stimulated, retinoic acid–inducible gene 1–mediated induction of interferon β, The Journal of Infectious Diseases 212(suppl_2) (2015) S277-S281.
[31] M.C. Jespersen, B. Peters, M. Nielsen, P. Marcatili, Bepipred-2.0: Improving sequence-based b-cell epitope prediction using conformational epitopes, Nucleic Acids Res. 45 (2017) W24-W29.
[32] B. Yao, L. Zhang, S. Liang, C. Zhang, Svmtrip: A method to predict antigenic epitopes using support vector machine to integrate tri-peptide similarity and propensity, PLoS One 7(9) (2012) e45152.
[33] H.R. Ansari, G.P. Raghava, Identification of conformational b-cell epitopes in an antigen from its primary sequence, Immunome Res 6(6) (2010).
[34] J.V. Kringelum, C. Lundegaard, O. Lund, M. Nielsen, Reliable b cell epitope predictions: Impacts of method development and improved benchmarking, PLoS Comput Biol. 8(12) (2012) e1002829.
[35] J.E. Larsen, O. Lund, M. Nielsen, Improved method for predicting linear b-cell epitopes., Immunome Res 2(2) (2006).
[36] J.V. Ponomarenko, P.E. Bourne, Antibody-protein interactions: Benchmark datasets and prediction tools evaluation, BMC Struct Biol 7(64) (2007).
[37] A.P. Haste, M. Nielsen, O. Lund, Prediction of residues in discontinuous b-cell epitopes using protein 3d structures, Protein Sci 15 (2006) 2553-2567.
[38] A. Fiser, R.K. Do, A. Sali, Modeling of loops in protein structures, Protein Sci 9 (2000) 1753-1773.
[39] M.A. Marti-Renom, A. Stuart, A. Fiser, R. Sanchez, F. Melo, A. Sali, Comparative protein structure modeling of genes and genomes, Annu. Rev. Biophys. Biomol. Struct. 29 (2000) 291-325.
[40] A. Sali, T.L. Blundell, Comparative protein modelling by satisfaction of spatial restraints, J. Mol. Biol. 234 (1993) 779-815.
[41] B. Webb, A. Sali, Comparative protein structure modeling using modeller, Current protocols in bioinformatics 54, John Wiley & Sons, Inc.2016.
[42] R.A. Laskowski, M.W. MacArthur, D.S. Moss, J.M. Thornton, Procheck - a program to check the stereochemical quality of protein structure, J. App. Cryst. 26 (1993) 283-291.
[43] R.A. Laskowski, J.A. Rullmannn, M.W. MacArthur, R. Kaptein, J.M. Thornton, Aqua and procheck-nmr: Programs for checking the quality of protein structures solved by nmr, J. Biomol. NMR 8 (1996) 477-486.
[44] J.U. Bowie, R. Lüthy, D. Eisenberg, A method to identify protein sequences that fold into a known three-dimensional structure, Science 253(5016) (1991) 164-170.
[45] R. Lüthy, J.U. Bowie, D. Eisenberg, Assessment of protein models with three-dimensional profiles, Nature 356(6364) (1992) 83-85.
[46] R.V. Honorato, P.I. Koukos, B. Jimenez-Garcia, A. Tsaregorodtsev, M. Verlato, A. Giachetti, A. Rosato, A.M.J.J. Bonvin, Structural biology in the clouds: The wenmr-eosc ecosystem, Frontiers Mol. Biosci. 8(729513) (2021) 1-7.
[47] G.C.P. van Zundert, J.P.G.L.M. Rodrigues, M. Trellet, C. Schmitz, P.L. Kastritis, E. Karaca, A.S.J. Melquiond, M. van Dijk, S.J. de Vries, A.M.J.J. Bonvin, The haddock2.2 webserver: User-friendly integrative modeling of biomolecular complexes, J. Mol. Biol. 428(4) (2016) 720-725.
[48] E. Krissinel, Stock-based detection of protein oligomeric states in jspisa, Nucleic Acids Res. 43(W1) (2015) W314-W319.

[49] A. Vangone, A.M.J.J. Bonvin, Contact-based prediction of binding affinity in protein-protein complexes, eLife 4 (2015) e07454.
[50] L. Xue, J. Rodrigues, P. Kastritis, A.M.J.J. Bonvin, A. Vangone, Prodigy: A web-server for predicting the binding affinity in protein-protein complexes, Bioinformatics 32(23) (2016) 3676-3678.
[51] F. Chen, H. Liu, H.Y. Sun, P.C. Pan, Y.Y. Li, D. Li, T.J. Hou, Assessing the performance of the mm/pbsa and mm/gbsa methods. 6. Capability to predict protein-protein binding free energies and re-rank binding poses generated by protein-protein docking, Physical Chemistry Chemical Physics 18(18) (2016) 22129-22139.
[52] T.J. Hou, J.M. Wang, Y.Y. Li, W. Wang, Assessing the performance of the mm/pbsa and mm/gbsa methods: I. The accuracy of binding free energy calculations based on molecular dynamics simulations, J. Chem. Inf. Model. 51(1) (2011) 69-82.
[53] H.Y. Sun, Y.Y. Li, S. Tian, L. Xu, T.J. Hou, Assessing the performance of mm/pbsa and mm/gbsa methods. 4. Accuracies of mm/pbsa and mm/gbsa methodologies evaluated by various simulation protocols using pdbbind data set, Physical Chemistry Chemical Physics 16(31) (2014) 16719-16729.
[54] G.Q. Weng, E.C. Wang, Z. Wang, H. Liu, D. Li, F. Zhu, T.J. Hou, Hawkdock: A web server to predict and analyze the structures of protein-protein complexes based on computational docking and mm/gbsa., Nucleic Acids Res. 47(W1) (2019) W322-W330.
[55] J.A. Maier, C. Martinez, K. Kasavajhala, L. Wickstrom, K.E. Hauser, C. Simmerling, Ff14sb: Improving the accuracy of protein side chain and backbone parameters from ff99sb, J. Chem. Theory Comput 11(8) (2015) 3696-3713.
[56] D.A. Case, I.Y. Ben-Shalom, S.R. Brozell, D.S. Cerutti, T.E. Cheatham, III, V.W.D. Cruzeiro, T.A. Darden, R.E. Duke, D. Ghoreishi, M.K. Gilson, H. Gohlke, A.W. Goetz, D. Greene, R. Harris, Amber 2018, University of California, San Francisco, 2018.
[57] S. Genheden, U. Ryde, The mm/pbsa and mm/gbsa methods to estimate ligand-binding affinities, Expert Opin Drug Discov 10(5) (2015) 449-461.
[58] E.F. Pettersen, T.D. Goddard, C.C. Huang, G.S. Couch, D.M. Greenblatt, E.C. Meng, T.E. Ferrin, Ucsf chimera--a visualization system for exploratory research and analysis, J Comput Chem 25(13) (2004) 1605-1612.
[59] L. Schrödinger, The pymol molecular graphics system. , 2010.
[60] D.W. Leung, N.D. Ginder, D.B. Fulton, J. Nix, C.F. Basler, R.B. Honzatko, G.K. Amarasinghe, Structure of the ebola vp35 interferon inhibitory domain, PNAS 106(2) (2009) 411-416.
[61] D.W. Leung, K.C. Prins, D.M. Borek, M. Farahbakhsh, J.M. Tufariello, P. Ramanan, J.C. Nix, L.A. Helgeson, Z. Otwinowski, R.B. Honzatko, C.F. Basler, G.K. Amarasinghe, Structural basis for dsrna recognition and interferon antagonism by ebola vp35, Nat. Struct. Mol. Biol. 17 (2010) 165-172.
[62] Y. Liu, A code within the genetic code: Codon usage regulates co-translational protein folding, Cell Communication and Signaling 18(1) (2020) 145.
[63] E. Angov, C.J. Hillier, R.L. Kincaid, J.A. Lyon, Heterologous protein expression is enhanced by harmonizing the codon usage frequencies of the target gene with those of the expression host, PLOS ONE 3(5) (2008) e2189.
[64] T. Dashivets, J. Stracke, S. Dengl, A. Knaupp, J. Pollmann, J. Buchner, T. Schlothauer, Oxidation in the complementarity-determining regions differentially influences the properties of therapeutic antibodies, mAbs 8(8) (2016) 1525-1535.
[65] A.L. Marschall, S. Dübel, T. Böldicke, Specific in vivo knockdown of protein function by intrabodies, mAbs 7(6) (2015) 1010-1035.

Fig. 1. Monoclone selection from naïve phage display library. (a) Polyclonal ELISA for two rounds of panning against rVP35 showed higher signal on rVP35 coated well compared to the background control well coated with BSA. (b) Several hits of monoclonal antibodies against rVP35 were demonstrated and presented in the heatmap as signal over noise (S/N) ratio. Clone with higher S/N is showed in darker colour. H5 and H11 were positive control, H6 and H12 were negative control of the ELISA. For both experiments, the absorbance reading at 405 nm was recorded after 30 min of incubation in dark.

Fig. 2. Coomassie Blue-stained SDS-PAGE of purified anti-VP35 A2, A5 and G3 expressed in (a,b) *E. coli* and (c) *L. tarentolae*. The band of the scFvs were approximately 35 kDa. M represents Opti-Protein XL Marker (abm); FT, flow-through of crude lysate passed through Ni-NTA resin; E, elution fraction; ctrl, in-house scFv produced from *E. coli*.

Fig. 3. The binding properties of clone A2, A5 and G3 to rVP35 on *in vitro* ELISA assay. (a) The clones expressed and extracted from *E. coli* showed different level of binding activity. A2 and A5 showed stronger binding signal compared to G3. All clones showed specificity towards rVP35 compared to other proteins such as BSA, ubiquitin, EGFP and HSP16.3. 5 µg of protein was coated and 10 µg of scFv was used for binding. Titration curves of the clones expressed in (b) *E. coli* and (c) *L. tarentolae* were also tested. For all clones, the binding signal increase when the amount of the scFv increase. The amount of rVP35 coated was kept constant at 1 µg. All data were plotted as mean of triplicate. Error bars indicate the mean ± SD of three independent ELISA.

Fig. 4. Inhibition effect of A2, A5 and G3 on VP35 as tested in luciferase reporter gene assay. EV represented negative control transfected with empty vector pcDNA3 only, VP35 represented positive control transfected with pcDNA3-VP35 only. The relative light units (RLU) of Luciferase signal were normalized to Renilla luciferase and over unstimulated

controls. Each assay was performed in triplicate. Results were presented as folds of IFN promoter induction over the empty vector and plotted as mean and standard deviation of replicates with GraphPad Prism 6.01. Error bars indicate the mean ± SD of two independent experiments. *P< 0.05 and **P< 0.01, two-tailed unpaired Student's t-test (Table S1).

Fig. 5. (a) The average conformation of A2-VP35 obtained from the last 10 ns of MD simulation. Green and yellow surfaces represent A2 and VP35, respectively. (b) Interactions of A2 heavy chain CDR2 (green ribbon and stick presentation) with VP35 (yellow ribbon and surface presentation). (c) Interactions of heavy chain CDR3 and, light chain CDR1 and CDR3 A2 (green ribbon and stick presentation) with VP35 yellow ribbon and surface presentation). Only A2 CDR hotspot residues with ΔG_{total} < -1 kcal/mol were shown here. Figure is prepared using PyMol [59].

Fig. 6. Structure alignment of anti-VP35 clones A2, A5 and G3 (a) Structure comparison between A2 and A5, in green and yellow ribbon and surface presentation, respectively. (b) Structure comparison between A2 and G3 in green and orange ribbon and surface presentation, respectively. Labelled residues indicate the locations of the same residue between scFv clones. The residues are numbered according to A2 clone. The locations of the hotspot residues in A5 and G3 were similar to the A2 clone. Figure is prepared using PyMol [59].

List of Tables

Table 1. V(D)J gene analysis of the anti-VP35 clones.

Clone	Heavy chain			Light chain	
	V-gene	D-gene	J-gene	V-gene	J-gene
A2	IGHV3-49*03 F	IGHD2-8*02 F	IGHJ5*02 F	IGKV2-28*01 F/ IGKV2D-28*01 F	IGKJ2*01 F
A5	IGHV3-13*01 F	IGHD3-22*01 F	IGHJ2*01 F	IGKV2-28*01 F/ IGKV2D-28*01 F	IGKJ2*01 F
G3	IGHV4-34*01 F	IGHD3-10*01 F	IGHJ6*02 F	IGLV3-9*01 F	IGLJ2*01 F/ IGLJ3*01 F/ IGLJ3*02 F

Table 2. Prediction of potential epitope regions in C-terminal IID of VP35 using five different servers. An epitope is identified from the consensus of at least four servers predicted a residue as an epitope.

Residue	215 GKPDISAKDL	225 RNIMYDHLPG	235 EGTAFHQLSQ	245 VICKLGKDSN	255 SLDIIHAEFQ	265 ASLAEGDSPQ	275 CALIQITKRV
BepiPred-2.0	-------*--	------****	**--------	------****	***-------	---*******	-------***
SVMTrip	---*******	*******---	---*****	**********	--********	******----	---*******
IEDB	-------*--	------****	***-------	------****	***-------	---*******	-------***
CBTope	**********	**-----*--	--*-------	********--	---***----	-------*--	--*****---
Discotope	****-*----	----------	----------	---------*	--*-------	-----*----	----------
Consensus	-------*--	------**--	----------	------**-*	--*-------	-----*----	----------

Residues	285 PIFQDAAPPV	295 IHPSRGPIP	305 RACQKSLRPV	315 PPSPKIDRGW	325 VCVFQLQDGK	335 TLGLKI
BepiPred-2.0	******----	**-*****	**********	********--	------****	***---
SVMTrip	*******---	---*******	********--	----------	**********	****--
IEDB	******-*--	---*******	**********	********--	------****	***---
CBTope	-------**-	--*-****--	*-*-*****-	*******---	-*---*---*	**-*--
Discotope	----*-----	*-****----	*---*---*-	***-------	----******	*-----
Consensus	----*-----	---******-	*-*-*****-	***-------	------****	**----

Table 3. MMGBSA and MMPBSA binding free energy calculations (ΔG) between scFvs (A2, A5 and G3) and VP35 using the last 10 ns of molecular dynamics simulation. Data was represented in mean ± SD.

	MMGBSA (ΔG; kcal/mol)			MMPBSA (ΔG; kcal/mol)		
scFv	**A2**	**A5**	**G3**	**A2**	**A5**	**G3**
VDWAALS	-71.55 ± 6.62	-62.75± 6.03	-50.15± 4.29	-71.55 ± 6.62	-62.75± 6.03	-50.15± 4.29
EEL	64.36 ± 37.16	-583.41± 43.23	-196.15± 33.49	64.36 ± 37.16	-583.41± 43.23	-196.15± 33.49
$EGB_{(MMGBSA)}$ / $EPB_{(MMPBSA)}$	5.96 ± 36.59	605.08± 37.92	240.99± 32.31	-16.26 ± 36.79	603.48± 38.50	222.17± 32.33
$ESURF_{(MMGBSA)}$ / $ENPOLAR_{(MMPBSA)}$	-9.36 ± 0.91	-10.91± 0.60	-7.02± 0.60	-8.39 ± 0.69	-8.67± 0.43	-5.92± 0.39
ΔG_{gas}	-7.19 ± 38.49	-646.15± 42.08	-246.30± 35.14	-7.19 ± 38.49	-646.15± 42.08	-246.30± 35.14
ΔG_{solv}	-3.39 ± 36.19	594.17± 37.64	233.96± 31.86	-25.15 ± 36.61	594.81± 38.31	216.24± 32.08
ΔG Total	-10.58 ± 5.28	-51.99± 8.37	-12.33± 5.24	-32.34 ± 7.66	-51.34± 10.04	-30.05± 7.37

Note: VDWAALS represents van der Waals energy of complex, EEL represents electrostatic energy of complex, EPB/EGB represents electrostatic energy contributed to solvation free energy, ESURF/ENPOLAR represents non-polar energy contributed to solvation free energy.

Table 4. Computational alanine scanning of A2 CDR for hotspot residues identification for the interaction with VP35. The analysis was performed using UCSF Chimera version 1.15 [56]. Computational alanine scanning was calculated on CDR residues in the last 10 ns of A2-VP35 MD simulation.

A2	CDR Residue	Alanine scanning, $\Delta\Delta G_{Total}$ (kcal/mol)	
		MMGBSA	MMPBSA
Heavy chain	1	-0.05	-0.86
Heavy chain	2	-0.14	-0.92
Heavy chain	3	-6.64	-2.36
	T99	0.00	0.00
	R100	0.09	0.59
	Y101	-0.05	0.17
	V103	0.02	0.00
	P105	-0.40	0.08
	Y106	-6.56	-2.13
	Q107	0.27	-0.06
	P108	-0.01	-0.03
	R109	0.13	0.22
	E110	-0.02	-0.70
	N111	0.00	0.02
	W112	-0.08	0.03
	F113	-0.02	0.06
	D114	-0.03	-0.53
	P115	0.00	-0.07
Light chain	1	-6.42	-4.72
	Q180	-0.26	-0.33
	S181	-0.04	0.05
	L182	0.02	-0.06
	L183	-0.02	-0.01
	H184	-2.78	-2.17
	S185	0.28	0.02
	N186	-0.19	-0.16
	Y188	-0.04	-0.08
	N189	0.01	0.00
	Y190	-3.40	-1.99
Light chain	2	-0.02	-0.12
Light chain	3	-1.54	-0.22

$\Delta\Delta G_{Total} = \Delta G_{WT} - \Delta G_{mutant}$

Table 5. Pairwise decomposition energies (ΔG) of scFv-VP35 complex by MMGBSA and MMPBSA using the last 10 ns of MD simulation. Only the CDR within scFv was calculated.

	MMGBSA (ΔG; kcal/mol)										
Chain	**A2 CDR Residue**	**ΔG_{Total}**	**ΔG_{Side}**	**ΔG_{Bb}**	**A5 CDR Residue**	**ΔG_{Total}**	**ΔG_{Side}**	**ΔG_{Bb}**	**G3 CDR Residue**	**ΔG_{Total}**	**ΔG_{Side}**	**ΔG_{Bb}**
Heavy	1	-0.04	-0.06	0.04	1	-24.62	-8.98	-15.62	1	-8.90	-6.78	-2.09
	G26	0.00	0.00	0.00	G26	-0.01	-0.00	-0.00	G26	-0.01	-0.01	-0.00
	F27	0.00	0.00	0.00	F27	-0.06	-0.02	-0.03	E27	-0.62	-0.60	-0.02
	T28	0.00	0.00	0.00	T28	-0.29	-0.20	-0.08	S28	-0.28	-0.27	-0.00
	F29	0.00	0.00	0.00	F29	-0.12	-0.09	-0.03	F29	-0.01	-0.02	0.01
	G30	0.00	-0.01	0.00	S30	-2.91	-1.73	-1.18	S30	-1.00	-1.04	0.04
	D31	-0.03	-0.05	0.03	R31	-3.88	-2.27	-1.62	G31	-1.76	-1.43	-0.32
	Y32	0.00	0.00	0.00	S32	0.09	-0.26	0.35	Y32	-2.02	-1.88	-0.13
	A33	0.00	0.00	0.01	D33	-17.46	-4.42	-13.04	Y33	-3.22	-1.54	-1.67
Heavy	2	-24.57	-13.37	-11.13	2	-16.43	-15.15	-1.24	2	-0.97	-0.87	-0.08
	I51	-0.01	-0.05	0.05								
	R52	-1.73	-1.48	-0.24								
	S53	-0.04	-0.02	-0.01								
	K54	-0.11	-0.04	-0.07	I51	-0.74	-0.25	-0.49	I51	-0.01	-0.02	0.02
	A55	-0.77	-0.70	-0.06	G52	-1.47	-1.40	-0.07	N52	-0.48	-0.46	-0.02
	Y56	-8.89	-3.82	-5.07	T53	-3.54	-3.38	-0.16	Q53	-0.36	-0.31	-0.04
	G57	-3.97	-2.13	-1.83	G54	-1.64	-1.44	-0.20	S54	-0.08	-0.04	-0.03
	G58	-6.24	-2.96	-3.28	G55	-0.19	-0.15	-0.03	G55	0.00	0.00	-0.00
	T59	-1.43	-0.95	-0.47	D56	-8.72	-8.43	-0.28	S56	-0.05	-0.03	-0.01
	T60	-1.37	-1.21	-0.15	T57	-0.12	-0.10	-0.02	T57	-0.01	-0.01	-0.00
Heavy	3	-10.44	-6.18	-4.23	3	-34.71	-30.22	-4.42	3	-34.17	-27.85	-6.26
	T99	0.00	0.00	0.00					A96	0.01	-0.00	0.01
	R100	0.02	0.04	-0.01	A96	0.05	0.02	0.03	R97	0.21	0.19	0.03
	Y101	-0.08	-0.04	-0.03	R97	0.37	0.12	0.25	V98	0.14	0.05	0.10

	G102	0.00	-0.01	0.01	E98	-15.71	-12.72	-2.99	V99	-0.19	-0.32	0.13
	V103	-0.17	-0.16	0.00	M99	-0.82	-1.05	0.24	Q100	-7.78	-6.64	-1.13
	G104	-0.01	-0.03	0.01	V100	-5.14	-3.92	-1.21	G101	-1.02	-1.10	0.09
	P105	-0.44	-0.21	-0.23	D101	-3.03	-2.67	-0.34	V102	-2.89	-2.36	-0.53
	Y106	-9.42	-5.60	-3.82	Y102	-0.57	-0.4	-0.16	Y103	-5.31	-5.13	-0.17
	Q107	-0.24	-0.12	-0.12	E103	-3.50	-3.45	-0.05	Y104	-8.11	-7.08	-1.02
	P108	-0.04	-0.02	-0.02	S104	-0.08	-0.06	-0.02	Y105	-8.53	-4.90	-3.63
	R109	0.02	0.04	-0.02	S105	-0.00	-0.00	0.00	Y106	-0.33	-0.24	-0.08
	E110	-0.02	-0.04	0.01	G106	0.04	0.01	0.03	G107	-0.09	-0.07	-0.02
	N111	0.00	0.00	0.00	W107	0.08	0.10	-0.01	M108	-0.03	-0.02	-0.01
	W112	-0.04	-0.02	-0.02	H108	-4.93	-4.89	-0.03	D109	-0.25	-0.22	-0.03
	F113	-0.01	0.00	0.00	F109	-1.16	-1.03	-0.13	V110	-0.01	-0.01	0.00
	D114	-0.01	-0.02	0.01	D110	-0.29	-0.25	-0.04				
	P115	0.00	0.00	0.00	L111	-0.02	-0.02	0.00				
Light	1	-10.96	-6.99	-3.95	1	-9.65	-8.51	-1.16	1	-0.54	-0.40	-0.12
	Q180	-0.76	-0.75	0.00	K176	0.06	0.05	0.01	N174	-0.04	-0.03	-0.01
	S181	-0.05	-0.06	0.01	S177	-0.01	-0.01	-0.00	I175	0.01	-0.01	0.01
	L182	-0.09	-0.08	0.00	L178	-0.02	-0.02	0.00	G176	-0.13	-0.12	-0.01
	L183	-0.04	-0.04	0.00	L179	-0.01	-0.01	0.00	G177	-0.11	-0.09	-0.02
	H184	-4.41	-3.31	-1.09	N180	-1.11	-0.82	-0.29	K178	-0.03	0.02	-0.05
	S185	-0.21	-0.15	-0.06	S181	-0.19	-0.16	-0.03	N179	-0.24	-0.19	-0.04
	N186	-0.60	-0.37	-0.23	D182	-6.91	-6.30	-0.61				
	G187	-0.01	0.00	0.00	G183	-0.03	-0.02	-0.01				
	Y188	-0.17	-0.10	-0.06	Y184	-0.37	-0.35	-0.02				
	N189	0.03	0.02	0.01	N185	0.01	0.00	0.01				
	Y190	-4.66	-2.14	-2.52	Y186	-1.11	-0.89	-0.22				
Light	2	-0.03	-0.02	-0.02	2	-0.15	-0.14	-0.00	2	-8.35	-8.21	-0.14
	L208	-0.03	-0.02	-0.01	L204	-0.15	-0.14	0.00	A197	-1.64	-1.64	0.01
	G209	0.00	0.00	0.00	G205	0.00	0.00	0.00	D198	-6.38	-6.25	-0.13
	S210	0.00	0.00	0.00	S206	0.00	0.00	0.00	S199	-0.33	-0.32	-0.01
Light	3	-14.25	-12.96	-1.25	3	-20.67	-19.78	-0.871	3	-0.69	-0.58	-0.08
	M247	0.01	0.00	0.01	M243	-0.00	-0.01	0.00	Q236	0.01	-0.00	0.02

	Q248	-0.04	-0.08	0.04	Q244	0.03	0.02	0.02	V237	-0.01	-0.01	0.00
	A249	-0.43	-0.45	0.03	A245	-0.18	-0.19	0.01	W238	-0.52	-0.43	-0.09
	L250	-6.62	-6.42	-0.19	L246	-1.07	-1.05	-0.02	H239	-0.05	-0.04	-0.01
	Q251	-4.03	-3.91	-0.12	E247	-11.86	-11.76	-0.10	S240	-0.07	-0.06	-0.01
	T252	-2.51	-1.63	-0.88	T248	-7.33	-6.71	-0.62	S241	-0.03	-0.02	-0.00
	P253	0.01	-0.06	0.07	P249	-0.04	0.06	-0.1	A242	-0.02	-0.01	0.00
	P254	-0.53	-0.34	-0.18	Y250	-0.21	-0.14	-0.07	V243	-0.00	-0.01	0.00
	Y255	-0.07	-0.05	-0.02	T251	-0.02	-0.01	-0.00	V244	-0.01	-0.01	-0.00
	T256	-0.04	-0.03	-0.02								

MMPBSA (ΔG; kcal/mol)

Chain	**A2 CDR Residue**	**ΔG_{Total}**	**ΔG_{Side}**	**ΔG_{Bb}**	**A5 CDR Residue**	**ΔG_{Total}**	**ΔG_{Side}**	**ΔG_{Bb}**	**G3 CDR Residue**	**ΔG_{Total}**	**ΔG_{Side}**	**ΔG_{Bb}**
Heavy	1	-0.42	-44.58	44.18	1	-24.03	-0.82	-23.18	1	-8.23	-72.25	64.06
	G26	0.00	-0.08	0.08	G26	-0.00	-0.34	0.34	G26	-0.02	-0.51	0.49
	F27	0.01	0.30	-0.29	F27	-0.00	1.13	-1.12	E27	-1.24	-62.18	60.94
	T28	-0.01	-0.36	0.35	T28	-0.42	-0.80	0.39	S28	-0.37	-1.12	0.76
	F29	-0.02	-0.84	0.82	F29	-0.35	-1.10	0.75	F29	-0.28	-1.45	1.18
	G30	-0.01	-1.04	1.03	S30	-1.79	-1.90	0.12	S30	-1.36	-2.99	1.63
	D31	-0.40	-43.53	43.13	D31	-1.84	81.34	-83.18	G31	-1.25	-0.95	-0.31
	Y32	0.02	0.11	-0.08	S32	0.19	-0.16	0.36	Y32	-1.31	-1.93	0.62
	A33	0.00	0.87	-0.86	D33	-19.83	-78.99	59.16	Y33	-2.40	-1.13	-1.26
Heavy	2	-18.47	105.67	-124.10	2	-14.88	-93.45	78.60	2	-0.72	4.67	-5.36
	I51	-0.12	0.57	-0.69								
	R52	0.08	66.86	-66.77								
	S53	0.01	0.39	-0.37								
	K54	0.21	48.27	-48.05	I51	-0.76	0.14	-0.89	I51	-0.11	-0.44	0.34
	A55	-0.46	0.97	-1.42	G52	-1.64	0.33	-1.97	N52	-0.39	3.15	-3.54
	Y56	-6.54	-4.85	-1.69	T53	-1.96	-1.31	-0.65	Q53	-0.22	-2.62	2.41
	G57	-3.57	1.40	-4.97	G54	-1.38	-0.60	-0.78	S54	0.01	2.83	-2.82
	G58	-4.91	-2.22	-2.68	G55	-0.48	0.77	-1.25	G55	0.05	1.27	-1.22
	T59	-0.96	0.14	-1.09	D56	-8.03	-91.49	83.47	S56	-0.12	-0.15	0.04

	T60	-2.21	-5.84	3.64	T57	-0.63	-1.29	0.66	T57	0.05	0.63	-0.57
Heavy	3	-6.33	7.74	-14.04	3	-36.46	-259.50	223.12	3	-28.47	-22.88	-5.53
	T99	-0.02	-0.72	0.70					A96	-0.01	-0.06	0.05
	R100	0.42	41.17	-40.75	A96	0.20	0.28	-0.08	R97	1.36	64.35	-62.98
	Y101	0.03	1.03	-1.00	R97	1.58	60.34	-58.76	V98	-0.06	-0.21	0.15
	G102	-0.02	-0.32	0.31	E98	-21.47	-90.80	69.33	V99	-0.17	-2.99	2.82
	V103	-0.24	-1.30	1.06	M99	-0.80	-1.36	0.56	Q100	-6.49	-7.98	1.49
	G104	0.05	0.53	-0.48	V100	-2.52	-1.86	-0.66	G101	-0.86	-0.23	-0.62
	P105	-0.38	0.78	-1.16	D101	-4.04	-81.73	77.70	V102	-2.58	-1.83	-0.74
	Y106	-6.13	-3.59	-2.53	Y102	-0.30	2.08	-2.38	Y103	-6.46	-9.10	2.64
	Q107	-0.20	-0.24	0.04	E103	-3.71	-83.09	79.38	Y104	-5.31	-2.17	-3.14
	P108	-0.04	-1.09	1.05	S104	0.30	2.31	-2.01	Y105	-6.09	-0.95	-5.13
	R109	0.88	45.55	-44.67	S105	0.10	1.64	-1.54	Y106	-0.21	2.25	-2.45
	E110	-0.41	-40.93	40.53	G106	0.10	-1.34	1.45	G107	-0.17	-2.01	1.84
	N111	0.00	-0.18	0.18	W107	-0.68	-0.85	0.17	M108	-0.05	-0.07	0.03
	W112	0.00	0.53	-0.52	H108	-3.66	-6.45	2.79	D109	-1.30	-60.86	59.56
	F113	0.03	0.55	-0.51	F109	0.27	1.70	-1.43	V110	-0.07	-1.02	0.95
	D114	-0.29	-33.41	33.12	D110	-1.68	-59.60	57.92				
	P115	-0.02	-0.62	0.60	L111	-0.13	-0.79	0.65				
Light	1	-9.79	-7.44	-2.34	1	-8.30	-46.30	38.04	1	0.33	43.68	-43.32
	Q180	-0.68	-0.92	0.24	K176	0.52	43.74	-43.22	N174	-0.08	-1.04	0.97
	S181	-0.17	-2.27	2.10	S177	-0.04	-1.26	1.22	I175	-0.19	-1.75	1.57
	L182	-0.11	-0.81	0.69	L178	-0.08	-1.42	1.33	G176	-0.20	-2.09	1.89
	L183	-0.15	-1.53	1.38	L179	0.00	-0.02	0.02	G177	-0.13	-1.79	1.66
	H184	-2.77	-2.23	-0.54	H180	-0.56	1.37	-1.93	K178	0.46	50.41	-49.95
	S185	-0.15	0.87	-1.02	S181	-0.12	0.16	-0.27	N179	0.46	-0.07	0.53
	N186	-0.47	0.58	-1.04	D182	-7.45	-88.77	81.32				
	G187	0.00	0.88	-0.88	G183	0.02	0.59	-0.57				
	Y188	-0.17	-1.00	0.83	Y184	-0.20	-0.22	0.03				
	N189	-0.04	-0.10	0.06	N185	-0.08	-0.30	0.22				
	Y190	-5.06	-0.89	-4.17	Y186	-0.31	-0.18	-0.13				
Light	2	0.10	2.03	-1.93	2	0.08	2.31	-2.22	2	-9.63	-69.75	60.14

	L208	0.06	0.92	-0.86	L204	0.02	1.00	-0.97	A197	-1.89	-1.36	-0.53
	G209	0.03	0.53	-0.50	G205	0.03	0.81	-0.77	D198	-7.89	-69.02	61.13
	S210	0.01	0.58	-0.57	S206	0.02	0.50	-0.48	S199	0.16	0.63	-0.47
Light	3	-12.84	-15.19	2.38	3	-19.46	-99.36	79.91	3	-0.67	-2.04	1.39
	M247	-0.03	0.06	-0.08	M243	-0.14	-1.23	1.09	Q236	-0.10	-0.11	0.02
	Q248	-0.43	-1.52	1.09	Q244	-0.06	-0.96	0.90	V237	0.03	0.99	-0.96
	A249	-0.51	-1.97	1.46	A245	-0.29	-1.81	1.52	W238	-0.38	0.72	-1.10
	L250	-6.46	-8.38	1.92	L246	-0.98	-3.63	2.64	H239	-0.05	-0.52	0.47
	Q251	-3.23	-1.90	-1.32	E247	-10.83	-83.45	72.63	S240	-0.12	-2.15	2.03
	T252	-1.26	-0.13	-1.12	T248	-6.93	-7.47	0.52	S241	-0.04	-0.16	0.12
	P253	-0.36	-0.56	0.20	P249	-0.14	-0.60	0.46	A242	-0.01	-0.59	0.57
	P254	-0.34	0.18	-0.52	Y250	-0.04	0.35	-0.38	V243	0.07	0.76	-0.69
	Y255	-0.03	-0.39	0.36	T251	-0.05	-0.57	0.52	V244	-0.07	-0.99	0.93
	T256	-0.20	-0.59	0.39								

ΔG_{Total} = total free binding energy for a residue
ΔG_{Side} = free binding energy of side chain with other residues in the complex
ΔG_{Bb} = free binding energy of backbone with other residues in the complex

Table 6. Sequence comparison of CDRs in scFv clones A5 and G3 against A2. The residues in CDR of A5 and G3 were aligned with A2 CDR to identify the sequence similarity between the CDRs. A5 and G3 heavy chain CDR2 and CDR3 in were similar to the respective A2 CDR, whereas A5 light chain CDR1 and CDR3 were similar to respective A2 CDR.

Clone	**Heavy chain**		
	CDR1	**CDR2**	**CDR3**
A5	GFTFSRSD	IGTGGDT	AREMVD YESSGWHFDL
		| | |	|
A2	GFTFGDYA	IRSKAYGGTT	TRYGVGPYQPRENWFDP
		| |	|
G3	GESFSGYY	INQSGST	ARVVQGVYYYYGMDV

Clone	**Light chain**		
	CDR1	**CDR2**	**CDR3**
A5	KSLLHSDGYNY	LGS	MQALETPYT
	| |		| |
A2	QSLLHSNGYNY	LGS	MQALQTPPYT
G3	NIGGKN	ADS	QVWHSSAVV

Note: The A2 hotspot residues (ΔG_{Total} < -1 kcal/mol) identified using pairwise decomposition analysis were in grey. "|" marked the residues in A5 and G3, which were identical to the hotspot residues in A2.

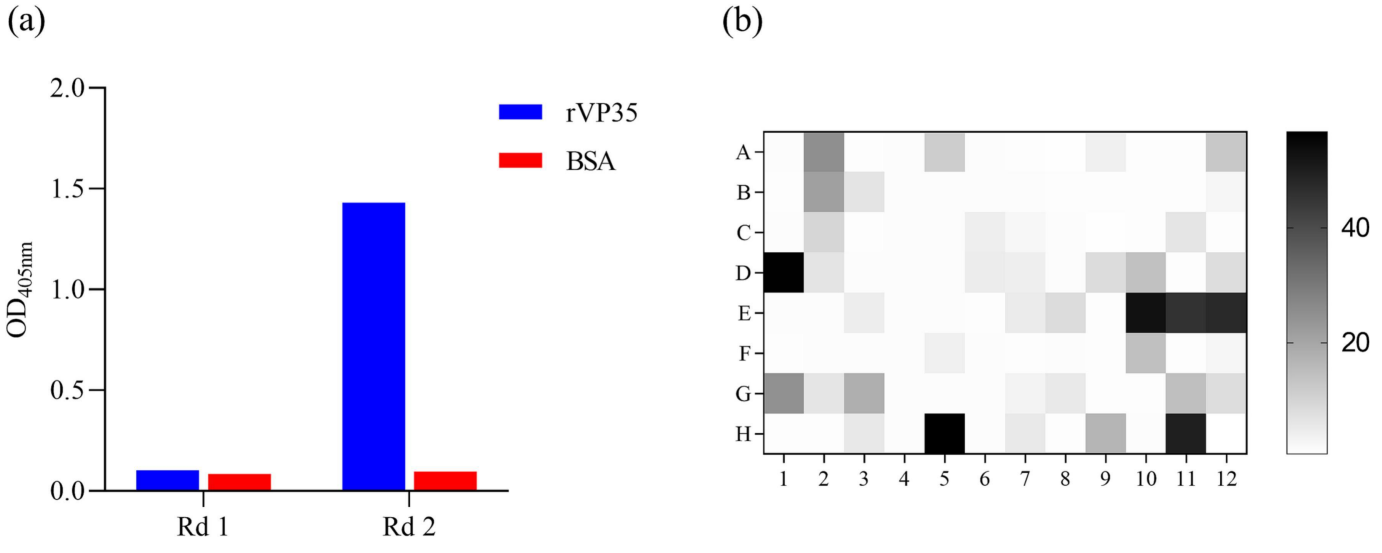
(a)
2.0
1.5
1.0
0.5
0.0
OD405nm
rVP35
BSA
Rd 1
Rd 2
(b)
A
B
C
D
E
F
G
H
1
2
3
4
5
6
7
8
9
10
11
12
40
20

Figure 1

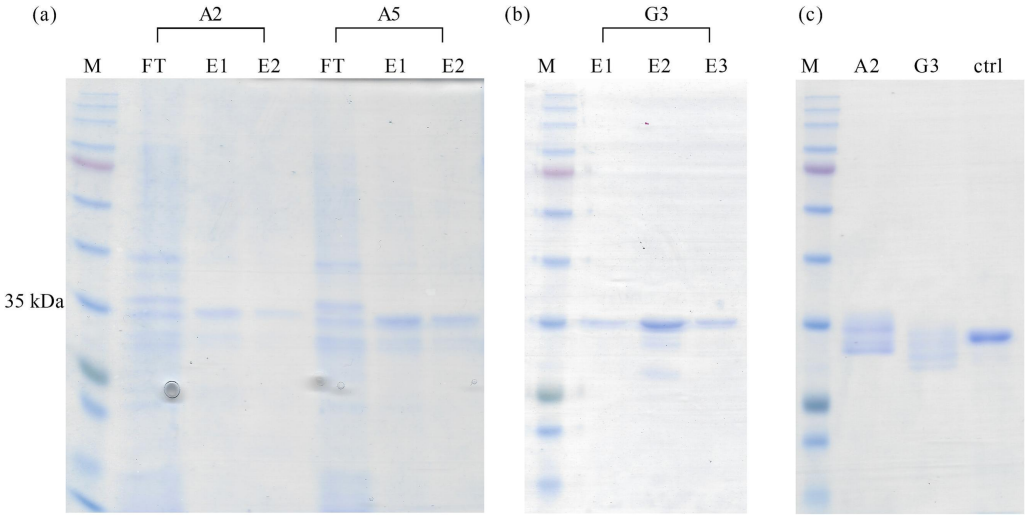

Figure 2

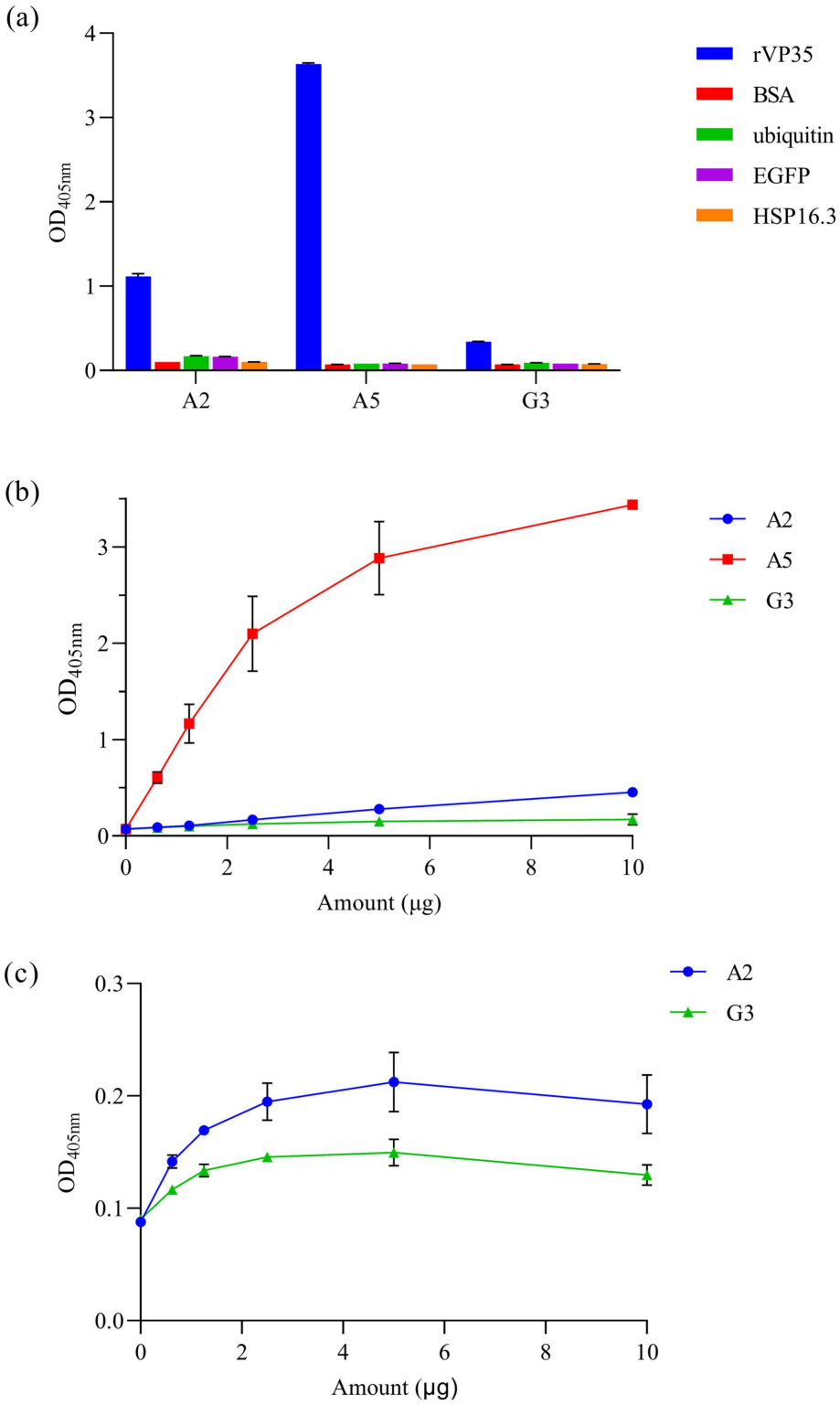
(a)
4
3
2
1
0
OD405nm
A2
A5
G3
rVP35
BSA
ubiquitin
EGFP
HSP16.3
(b)
3
2
1
0
OD405nm
0
2
4
6
8
10
Amount (μg)
A2
A5
G3
(c)
0.3
0.2
0.1
0.0
OD405nm
0
2
4
6
8
10
Amount (μg)
A2
G3

Figure 3

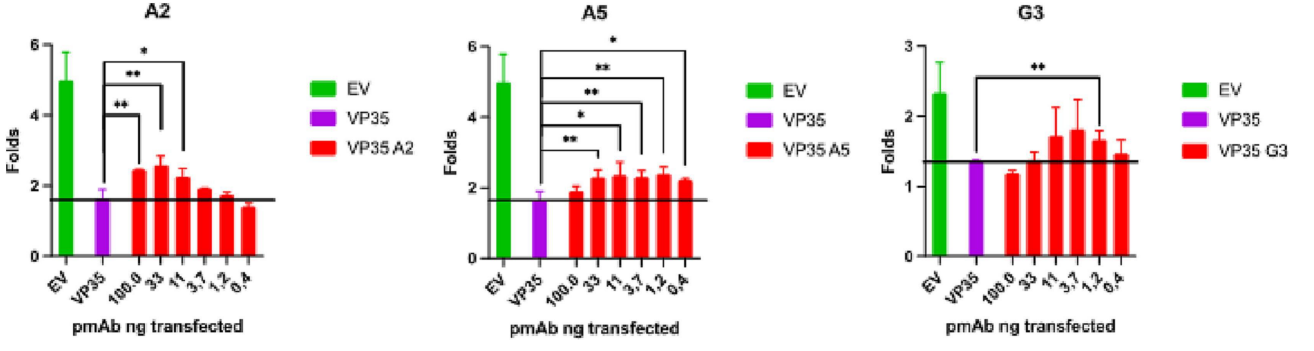
A2
Folds
6
4
2
0
*
**
**
EV
VP35
100.0
33
11
3,7
1,2
0,4
pmAb ng transfected
EV
VP35
VP35 A2
A5
Folds
6
4
2
0
*
**
**
*
**
EV
VP35
100.0
33
11
3,7
1,2
0,4
pmAb ng transfected
EV
VP35
VP35 A5
G3
Folds
3
2
1
0
**
EV
VP35
100.0
33
11
3,7
1,2
0,4
pmAb ng transfected
EV
VP35
VP35 G3

Figure 4

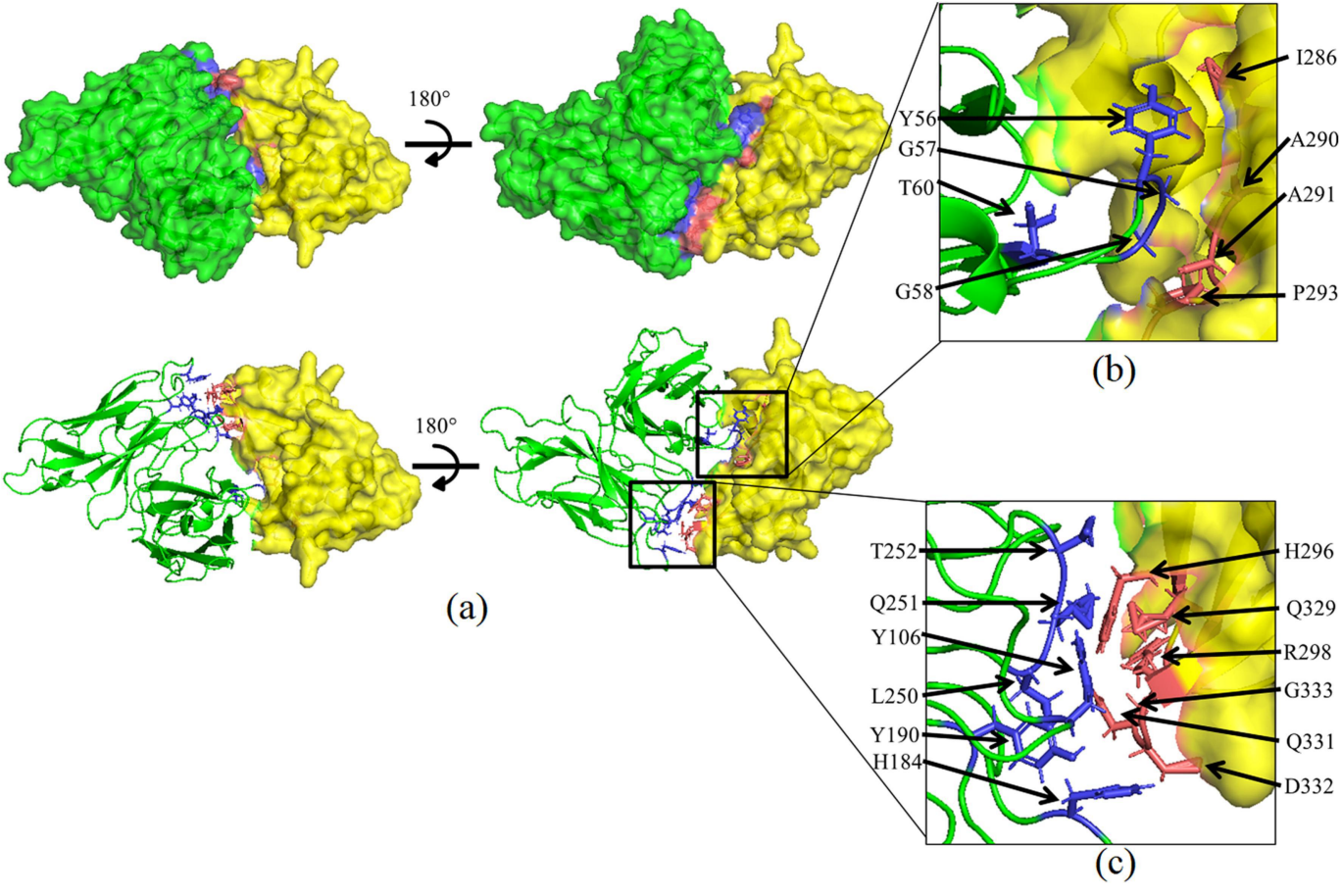
180°
180°
(a)
I286
Y56
A290
G57
T60
A291
G58
P293
(b)
T252
H296
Q251
Q329
Y106
R298
L250
G333
Y190
Q331
H184
D332
(c)

Figure 5

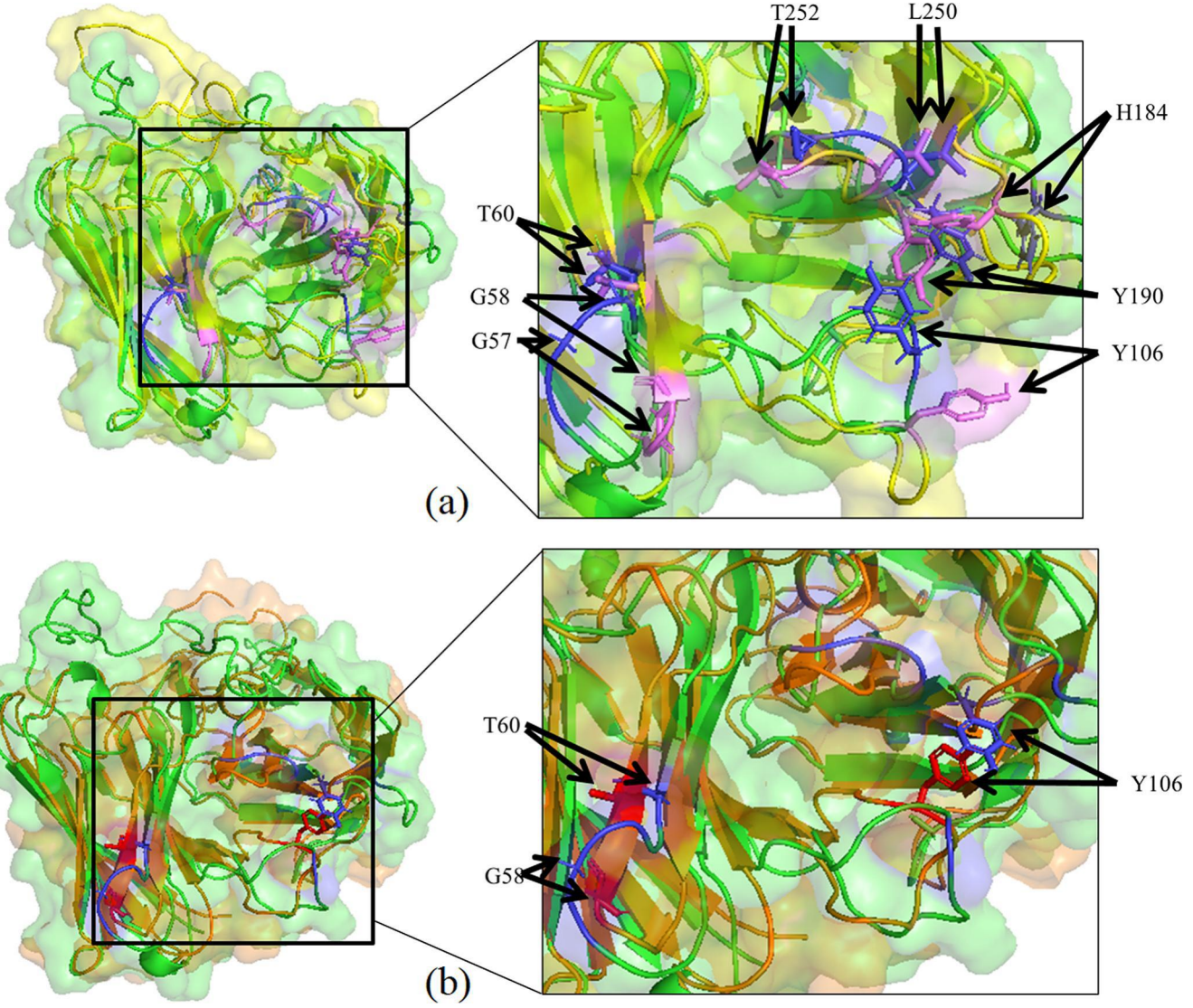

Figure 6